Two-dimensional Static Fields in Magnetoelectroelastic Laminates*

PAUL R. HEYLIGER,[1,†] FERNANDO RAMIREZ[1] AND ERNIAN PAN[2]

[1]*Department of Civil Engineering, Colorado State University, Fort Collins, CO 80523, USA*

[2]*Department of Mechanical Engineering, University of Akron, Akron, OH 44325, USA*

The two-dimensional behavior of laminated magnetoelectroelastic plates is investigated for two specific geometries: laminates under conditions of cylindrical bending and homogeneous plates under traction-free conditions. These plates are composed of a collection of elastic, piezoelectric, and magnetostrictive layers with perfect bonding between each interface. We investigate the through-thickness behavior of the five primary unknowns (the three displacements and the electric and magnetic potentials) under a variety of boundary conditions and aspect ratios using a discrete-layer theory. Results are compared with exact solutions for the case of cylindrical bending and finite element models for traction-free deformation. Excellent agreement is found between the approaches, and generalizations regarding global plate behavior are summarized.

Key Words: laminated, magnetostrictive, piezoelectric, cylindrical, bending, smart, adaptive, magnetoelectroelastic

INTRODUCTION

MAGNETOELECTROELASTIC laminates possess coupled field behavior between the elastic, electric, and magnetic field variables that depend strongly on the specific edge and surface conditions and the combination of the material parameters within the different layers. These laminates can contain three different types of materials: (1) elastic materials that possess physical relations between stress and strain fields and electric displacement and electric fields, but no coupling between the elastic and electric fields nor the elastic and magnetic fields; (2) piezoelectric materials that possess the same couplings as elastic materials but also possess coupling between the electric and elastic fields; and (3) magnetostrictive materials that possess the same couplings as elastic materials but also possess coupling between the magnetic and elastic fields. Problems involving coupled magnetoelectroelastic media are significantly more complex than the far more usual piezoelectric laminates (Tzou, 1993; Saravanos, 1999), and have been considered by Harshe et al. (1993), Nan (1994), and Benveniste (1995), and the three-dimensional behavior of magnetoelectroelastic laminates under simple support has been studied by Pan (2001) and Pan and Heyliger (2002). An exact solution for magnetoelectroelastic laminates in cylindrical bending has also been obtained by Pan and Heyliger (2002).

In this study, the basic through-thickness behavior of magnetoelectroelastic laminates is considered using an approximate discrete-layer representation of the three displacement components, the electric potential, and the magnetic potential. There are two primary objectives of this work. First, we determine the fundamental behavior of these five fields and the additional secondary fields of stress, electric displacement, and magnetic flux when these plates are subjected to mechanical, electric, or magnetic excitation. Second, we seek limits on the accuracy of theories that may be introduced to more efficiently model the behavior of these structural components while maintaining much of the accuracy of more complex approximate models. Two primary geometries are studied: the laminated plate under cylindrical bending, for which an exact solution exists (Pan and Heyliger, 2002), and the completely traction-free plate under surface potentials. Both problems are considered to develop initial estimates for the level of sensing and actuation that may be possible, and outline the limitations of various plate theories in modeling these novel components.

THEORY

Geometry and Governing Equations

We consider a laminated solid that is either very thin or infinitely long in the y-direction and composed of an arbitrary number of elastic, piezoelectric,

*Presented at ICAST 2002 (International Conference on Adaptive Structures and Technologies, Potsdam, Germany, October 7–9, 2002).

†Author to whom correspondence should be addressed.

1045-389X/04/9/10 0689–21 $10.00/0 DOI: 10.1177/1045389X04041652

or magnetostrictive layers. The laminate has dimensions L_x in the x-direction as has total thickness h, with individual layer thicknesses of h_1, h_2, and so on labeled from the bottom up. Each layer has the constitutive equations that can be expressed as (Harshe et al., 1993):

$$\begin{aligned} \sigma_i &= C_{ik}\gamma_k - e_{ki}E_k - q_{ki}H_k \\ D_i &= e_{ik}\gamma_k + \epsilon_{ik}E_k + d_{ik}H_k \\ B_i &= q_{ik}\gamma_k + d_{ik}E_k + \mu_{ik}H_k \end{aligned} \tag{1}$$

Here C_{ij}, ϵ_{ij}, and μ_{ij} are the components of elastic stiffness and dielectric and magnetic permittivity, respectively. The symbols σ_i, D_i, and B_i denote the components of stress, electric displacement, and magnetic flux, and γ_k, E_k, and H_k denote the components of linear strain, electric field, and magnetic field, respectively. The standard contraction in indices has been used here for the elastic variables (i.e. $\gamma_4 = \gamma_{23}$, etc.).

The components of strain, electric field, and magnetic field are related to the displacement field u_i, and the electric and magnetic potentials ϕ and ψ by the relations

$$\gamma_{ij} = \frac{1}{2}\left(\frac{\partial u_i}{\partial x_j} + \frac{\partial u_j}{\partial x_i}\right) \tag{2}$$

$$E_i = -\phi_{,i} \tag{3}$$

$$H_i = -\psi_{,i} \tag{4}$$

Within the laminate, the body force vector f_i and the free charge density ρ are given functions of position. Under these conditions, the equations of equilibrium, and the Gauss's laws for electrostatics and magnetism are given as

$$\sigma_{ij,j} + f_i = \rho u_{i,tt} \tag{5}$$

$$D_{i,i} = \rho_f \tag{6}$$

$$B_{i,i} = 0 \tag{7}$$

The nonzero terms for the rotated orthotropic property tensors for the materials used in this study can be expressed in matrix form as follows:

$$[C] = \begin{bmatrix} C_{11} & C_{12} & C_{13} & 0 & 0 & C_{16} \\ C_{12} & C_{22} & C_{23} & 0 & 0 & C_{26} \\ C_{13} & C_{23} & C_{33} & 0 & 0 & C_{36} \\ 0 & 0 & 0 & C_{44} & C_{45} & 0 \\ 0 & 0 & 0 & C_{45} & C_{55} & 0 \\ C_{16} & C_{26} & C_{36} & 0 & 0 & C_{66} \end{bmatrix}$$

$$[q] = \begin{bmatrix} 0 & 0 & 0 & q_{14} & q_{15} & 0 \\ 0 & 0 & 0 & q_{24} & q_{25} & 0 \\ q_{31} & q_{32} & q_{33} & 0 & 0 & q_{36} \end{bmatrix}$$

$$[e] = \begin{bmatrix} 0 & 0 & 0 & e_{14} & e_{15} & 0 \\ 0 & 0 & 0 & e_{24} & e_{25} & 0 \\ e_{31} & e_{32} & e_{33} & 0 & 0 & e_{36} \end{bmatrix}$$

$$[\epsilon] = \begin{bmatrix} \epsilon_{11} & \epsilon_{12} & 0 \\ \epsilon_{12} & \epsilon_{22} & 0 \\ 0 & 0 & \epsilon_{33} \end{bmatrix}$$

$$[d] = \begin{bmatrix} d_{11} & d_{12} & 0 \\ d_{12} & d_{22} & 0 \\ 0 & 0 & d_{33} \end{bmatrix}$$

$$[\mu] = \begin{bmatrix} \mu_{11} & \mu_{12} & 0 \\ \mu_{12} & \mu_{22} & 0 \\ 0 & 0 & \mu_{33} \end{bmatrix}$$

The specific values for each of the material parameters used for the examples presented later in this study are given in Table 1. Many of the nonzero terms in these matrices come only from a rotation of orthotropic properties about the z-axis. Also, the coupling coefficients d_{ik} are zero for the materials considered in this study, and the coupling between the electric and magnetic fields are therefore generated by the so-called product property that links strain generated by electric field with an induced magnetic field, and vice versa. However, they are easily included in this formulation.

Table 1. *Material properties and units for the three materials used in numerical examples.*

Parameter	$CoFeO_4$	$BaTiO_3$	PVDF
C_{11} (GPa)	286.0	166.0	238.0
C_{22}	286.0	166.0	23.6
C_{33}	269.5	162.0	10.6
C_{13}	170.5	78.0	4.4
C_{23}	170.5	78.0	2.15
C_{12}	173.0	77.0	6.43
C_{44}	45.3	43.0	1.92
C_{55}	45.3	43.0	2.19
C_{66}	56.5	44.5	3.98
e_{31} (C/m^2)	0.0	−4.4	−0.13
e_{32}	0.0	−4.4	−0.14
e_{33}	0.0	18.6	−0.28
e_{24}	0.0	11.6	−0.01
e_{15}	0.0	11.6	−0.01
q_{31} (N/Am)	580.3	0.0	0.0
q_{32}	580.3	0.0	0.0
q_{33}	699.7	0.0	0.0
q_{24}	550.0	0.0	0.0
q_{15}	550.0	0.0	0.0
ϵ_{11} ($10^{-9}\,C^2/Nm^2$)	0.080	11.2	11.0625
ϵ_{22}	0.080	11.2	10.6023
ϵ_{33}	0.093	12.6	10.6023
$d_{11} = d_{22} = d_{33}$	0.0	0.0	0.0
μ_{11} ($10^{-6}\,Ns^2/C^2$)	−590.0	5.0	5.0
μ_{22}	−590.0	5.0	5.0
μ_{33}	157.0	10.0	10.0

Variational Formulation

Following a formulation that is standard in variational methods of approximation (Reddy, 1984), we multiply the equations of equilibrium, Gauss's law, and Gauss's law for magnetism by arbitrary functions that physically represent a virtual displacement δu_i, a virtual electrostatic potential $\delta\phi$, and a virtual magnetic potential $\delta\psi$, respectively. We then integrate the result over the volume of our domain and set the result equal to zero. This results in

$$\int_V \delta u_i(\sigma_{ij,j} + f_i)dV = 0 \tag{8}$$

$$\int_V \delta\phi(D_{i,i} - \rho_f)dV = 0 \tag{9}$$

$$\int_V \delta\psi(B_{i,i})dV = 0 \tag{10}$$

Integrating these equations by parts and applying the divergence theorem yields

$$0 = \int_V \left(\sigma_{ij}\delta\epsilon_{ij} - \delta u_i f_i\right)dV - \oint_S \sigma_{ij}n_j\delta u_i dS \tag{11}$$

$$0 = \int_V \left(D_j\delta\phi_{,j} + \rho_f\delta\phi\right)dV - \oint_S D_j n_j\delta\phi dS \tag{12}$$

$$0 = \int_V B_j\delta\psi_{,j}dV - \oint_S B_j n_j\delta\psi dS \tag{13}$$

Substituting the governing constitutive equations into these equations yields the final weak form as

$$\begin{aligned}
0 = \int_V \Bigg\{ & \Bigg[C_{11}\frac{\partial u}{\partial x} + C_{13}\frac{\partial w}{\partial z} + C_{14}\frac{\partial v}{\partial z} + C_{16}\frac{\partial v}{\partial x} + e_{11}\frac{\partial\phi}{\partial x} \\
& + e_{31}\frac{\partial\phi}{\partial z} + q_{11}\frac{\partial\psi}{\partial x} + q_{31}\frac{\partial\psi}{\partial z}\Bigg]\frac{\partial\delta u}{\partial x} \\
& + \Bigg[C_{12}\frac{\partial u}{\partial x} + C_{23}\frac{\partial w}{\partial z} + C_{24}\frac{\partial v}{\partial z} + C_{26}\frac{\partial v}{\partial x} + e_{12}\frac{\partial\phi}{\partial x} \\
& + e_{32}\frac{\partial\phi}{\partial z} + q_{12}\frac{\partial\psi}{\partial x} + q_{32}\frac{\partial\psi}{\partial z}\Bigg]\frac{\partial\delta v}{\partial y} \\
& + \Bigg[C_{13}\frac{\partial u}{\partial x} + C_{33}\frac{\partial w}{\partial z} + C_{36}\frac{\partial v}{\partial x} + e_{33}\frac{\partial\phi}{\partial z} + q_{33}\frac{\partial\psi}{\partial z}\Bigg]\frac{\partial\delta w}{\partial z} \\
& + \Bigg[C_{14}\frac{\partial u}{\partial x} + C_{44}\frac{\partial v}{\partial z} + C_{45}\left(\frac{\partial u}{\partial z} + \frac{\partial w}{\partial x}\right) + e_{14}\frac{\partial\phi}{\partial x} + q_{14}\frac{\partial\psi}{\partial x}\Bigg]\frac{\partial\delta v}{\partial z} \\
& + \Bigg[C_{45}\frac{\partial v}{\partial z} + C_{55}\left(\frac{\partial u}{\partial z} + \frac{\partial w}{\partial x}\right) + e_{15}\frac{\partial\phi}{\partial x} + q_{15}\frac{\partial\psi}{\partial x}\Bigg]\left(\frac{\partial\delta u}{\partial z} + \frac{\partial\delta w}{\partial x}\right) \\
& + \Bigg[C_{16}\frac{\partial u}{\partial x} + C_{36}\frac{\partial w}{\partial z} + C_{66}\frac{\partial v}{\partial x} + e_{16}\frac{\partial\phi}{\partial x} + e_{36}\frac{\partial\phi}{\partial z} \\
& + q_{16}\frac{\partial\psi}{\partial x} + q_{36}\frac{\partial\psi}{\partial z}\Bigg]\frac{\partial\delta v}{\partial x} - (f_x\delta u + f_y\delta v + f_z\delta z)\Bigg\}dV \\
& - \oint_S \left(t_x\delta u + t_y\delta v + t_z\delta z\right)dS
\end{aligned} \tag{14}$$

$$\begin{aligned}
0 = \int_V \Bigg\{ & \Bigg[e_{11}\frac{\partial u}{\partial x} + e_{12}\frac{\partial v}{\partial y} + e_{14}\left(\frac{\partial v}{\partial z} + \frac{\partial w}{\partial y}\right) + e_{15}\left(\frac{\partial u}{\partial z} + \frac{\partial w}{\partial x}\right) \\
& + e_{16}\left(\frac{\partial u}{\partial y} + \frac{\partial v}{\partial x}\right) - \epsilon_{11}\frac{\partial\phi}{\partial x} - \epsilon_{12}\frac{\partial\phi}{\partial y} - d_{11}\frac{\partial\psi}{\partial x} - d_{12}\frac{\partial\psi}{\partial y}\Bigg]\frac{\partial\delta\phi}{\partial x} \\
& + \Bigg[e_{21}\frac{\partial u}{\partial x} + e_{22}\frac{\partial v}{\partial y} + e_{24}\left(\frac{\partial v}{\partial z} + \frac{\partial w}{\partial y}\right) + e_{25}\left(\frac{\partial u}{\partial z} + \frac{\partial w}{\partial x}\right) \\
& + e_{26}\left(\frac{\partial u}{\partial y} + \frac{\partial v}{\partial x}\right) - \epsilon_{12}\frac{\partial\phi}{\partial x} - \epsilon_{22}\frac{\partial\phi}{\partial y} - d_{12}\frac{\partial\psi}{\partial x} - d_{22}\frac{\partial\psi}{\partial y}\Bigg]\frac{\partial\delta\phi}{\partial y} \\
& + \Bigg[e_{31}\frac{\partial u}{\partial x} + e_{32}\frac{\partial v}{\partial y} + e_{33}\frac{\partial w}{\partial z} + e_{36}\left(\frac{\partial u}{\partial y} + \frac{\partial v}{\partial y}\right) \\
& - \epsilon_{33}\frac{\partial\phi}{\partial z} - d_{33}\frac{\partial\psi}{\partial z}\Bigg]\frac{\partial\delta\phi}{\partial z} - \rho_f\delta\phi\Bigg\}dV - \oint_S D_j n_j\delta\phi dS
\end{aligned} \tag{15}$$

$$\begin{aligned}
0 = \int_V \Bigg\{ & \Bigg[q_{11}\frac{\partial u}{\partial x} + q_{12}\frac{\partial v}{\partial y} + q_{14}\left(\frac{\partial v}{\partial z} + \frac{\partial w}{\partial y}\right) + q_{15}\left(\frac{\partial u}{\partial z} + \frac{\partial w}{\partial x}\right) \\
& + q_{16}\left(\frac{\partial u}{\partial y} + \frac{\partial v}{\partial x}\right) - d_{11}\frac{\partial\phi}{\partial x} - d_{12}\frac{\partial\phi}{\partial y} - \mu_{11}\frac{\partial\psi}{\partial x} - \mu_{12}\frac{\partial\psi}{\partial y}\Bigg]\frac{\partial\delta\psi}{\partial x} \\
& + \Bigg[q_{21}\frac{\partial u}{\partial x} + q_{22}\frac{\partial v}{\partial y} + q_{24}\left(\frac{\partial v}{\partial z} + \frac{\partial w}{\partial y}\right) + q_{25}\left(\frac{\partial u}{\partial z} + \frac{\partial w}{\partial x}\right) \\
& + q_{26}\left(\frac{\partial u}{\partial y} + \frac{\partial v}{\partial y}\right) - d_{12}\frac{\partial\phi}{\partial x} - d_{22}\frac{\partial\phi}{\partial y} - \mu_{12}\frac{\partial\psi}{\partial x} - \mu_{22}\frac{\partial\psi}{\partial y}\Bigg]\frac{\partial\delta\psi}{\partial y} \\
& + \Bigg[q_{31}\frac{\partial u}{\partial x} + q_{32}\frac{\partial v}{\partial y} + q_{33}\frac{\partial w}{\partial z} + q_{36}\left(\frac{\partial u}{\partial y} + \frac{\partial v}{\partial x}\right) \\
& - d_{33}\frac{\partial\phi}{\partial z} - \mu_{33}\frac{\partial\psi}{\partial z}\Bigg]\frac{\partial\delta\psi}{\partial z}\Bigg\}dV - \oint_S B_j n_j\delta\psi dS
\end{aligned} \tag{16}$$

Hence we do not seek direct solutions of the displacements and potentials to the governing differential equations, but rather approximate solutions to the weak form given in these equations. There are many different combinations of functions that could be used to approximate the independent unknowns and their variations, but we introduce an approach that allows for numerous simplified plate theories to be included as a special case while retaining the freedom to make the analysis as accurate as possible.

Discrete-Layer Approximation

Since the plate geometry is such that the length in y is either extremely thin or infinitely long, there is no dependence on this spatial variable in any of the five independent unknowns. Approximations to the three displacements, the electrostatic potential, and the magnetic potential are generated in terms of the global (x, z) coordinates, with the dependence of the displacements on the z coordinate separated from the functions in x. This allows for global functions in x and z that result in a subsequent reduction of the size of the computational problem. Hence approximations for the five unknown

field quantities are sought in the form (Pauley and Dong, 1976; Reddy, 1987)

$$
\begin{aligned}
u(x,z,t) &= \sum_{j=1}^{n} U_j(x)\Gamma_j^u(z) = \sum_{i=1}^{m}\sum_{j=1}^{n} U_{ji}(t)\Gamma_i^u(x)\Gamma_j^u(z)\\
v(x,z,t) &= \sum_{j=1}^{n} V_j(x)\Gamma_j^v(z) = \sum_{i=1}^{m}\sum_{j=1}^{n} V_{ji}(t)\Gamma_i^v(x)\Gamma_j^v(z)\\
w(x,z,t) &= \sum_{j=1}^{n} W_j(x)\Gamma_j^w(z) = \sum_{i=1}^{m}\sum_{j=1}^{n} W_{ji}(t)\Gamma_i^w(x)\Gamma_j^w(z)\\
\phi(x,z,t) &= \sum_{j=1}^{n} \Phi_j(x)\Gamma_j^\phi(z) = \sum_{i=1}^{m}\sum_{j=1}^{n} \Phi_{ji}(t)\Gamma_i^\phi(x)\Gamma_j^\phi(z)\\
\psi(x,z,t) &= \sum_{j=1}^{n} \Psi_j(x)\Gamma_j^\psi(z) = \sum_{i=1}^{m}\sum_{j=1}^{n} \Psi_{ji}(t)\Gamma_i^\psi(x)\Gamma_j^\psi(z)
\end{aligned}
\tag{17}
$$

The approximations for each of the five field quantities are constructed in such a way as to separate the dependence along the axis with that in the direction perpendicular to the plate axis. The reason for this is that the change in the material properties forces a break in the gradients of the displacements across an interface. This can be easily seen by considering the specialized case of elastostatic and electrostatics. In the former case, the shear stress must be continuous across an interface, but the shear modulus is different for two layers. Hence the shear strain must be different, implying changes in the slope of the displacement variables across the interface. Similar behavior is true for the electric displacement and magnetic flux. This character is crucially different from equivalent single layer theories, in which the fields through the thickness are generally assumed to have continuous derivatives across a dissimilar material interface. The loss of accuracy that is consistent with such an approximation is an open question for magneto-electroelastic laminates.

In the thickness direction, one-dimensional Lagrangian interpolation polynomials are used for $\Gamma_j(z)$ for each of the five variables. For the in-plane approximations (i.e. that in the x-direction), different types of approximations can be used for the one-dimensional functions $\Gamma_j(x)$. Power and Fourier series are used in the present study. For a laminate with n layers, $(n-1)$ is the number of subdivisions through the parallelepiped thickness (typically taken equal to or greater than the number of layers in the parallelepiped), and $U_{ji}, V_{ji}, W_{ji}, \Phi_{ji}$, and Ψ_{ji} are the values of the respective component at height j corresponding to the ith in-plane approximation function (Reddy, 1987).

Substituting these approximations into the weak form, collecting the coefficients of the variations of the displacements, and placing the results in matrix form yields the result

$$
\begin{bmatrix}
[K^{uu}] & [K^{uv}] & [K^{uw}] & [K^{u\phi}] & [K^{u\psi}]\\
[K^{vu}] & [K^{vv}] & [K^{vw}] & [K^{v\phi}] & [K^{v\psi}]\\
[K^{wu}] & [K^{wv}] & [K^{ww}] & [K^{w\phi}] & [K^{w\psi}]\\
[K^{\phi u}] & [K^{\phi v}] & [K^{\phi w}] & [K^{\phi\phi}] & [K^{\phi\psi}]\\
[K^{\psi u}] & [K^{\psi v}] & [K^{\psi w}] & [K^{\psi\phi}] & [K^{\psi\psi}]
\end{bmatrix}
\begin{Bmatrix} \{U\}\\ \{V\}\\ \{W\}\\ \{\Phi\}\\ \{\Psi\} \end{Bmatrix}
=
\begin{Bmatrix} \{f^u\}\\ \{f^v\}\\ \{f^w\}\\ \{f^\phi\}\\ \{f^\psi\} \end{Bmatrix}
\tag{18}
$$

The elements of each of these submatrices have a very specific form as a result of the pre-integration of the thickness dependence. The submatrices are in fact composed of smaller submatrices that consist of the fully-integrated thickness approximation functions multiplied by the various in-plane functions. We have shown the explicit form of each of these submatrices in the Appendix prior to the insertion of the specific discrete-layer approximations.

There are two key features of the structure of the final matrix statement. First, the submatrices related to the through-thickness approximations do not change for problems with different boundary conditions. They are fixed functions that remain the same regardless of what behavior is being represented in-plane (except for their relative contributions through their respective multiplying coefficient). Hence these submatrices are analytically preintegrated and fixed in our algorithm, eliminating this computational step. Second, we select linear Lagrangian interpolation polynomials for our approximations in z. This explicitly allows for a discontinuity of the derivatives of the functions across a discrete-layer interface. This type of approximation is selected because there is continuity of the primary unknowns u, v, w, ϕ, ψ as well as the secondary unknowns σ_{xz}, σ_{yz}, σ_{zz}, D_z, and B_z across a dissimilar material interface. Examining the constitutive equations, it is clear that if there is a jump in the numerical value of the elements of the constitutive tensors, there must be a concomitant discontinuity in the thickness-direction slope of the primary unknowns. Hence we enforce this behavior via the selection of our through-thickness basis functions. It is stressed that there are many acceptable choices for these basis functions, and those selected here are one combination of many that could alternatively be used.

NUMERICAL EXAMPLES AND DISCUSSION

We consider two geometries in this section to assess the level of accuracy of the discrete-layer model and determine the order of approximation necessary for reasonable results. The first example is the laminate

under simple support, a geometry that is very useful in that an exact solution is available with which to compare (Pan, 2002). The second geometry is the completely traction-free plate under the effects of applied surface potential leading to an imposed electric or magnetic field.

Three different materials are studied in the examples that follow. The first is the much-studied piezoelectric solid $BaTiO_3$, the second is the purely magnetostrictive material $CoFe_2O_4$, and the third is the piezoelectric polymer PVDF. The material properties for all of these solids are given in Table 1 along with the appropriate units for each (Berlincourt et al., 1964; Tashiro et al., 1981).

Simply-Supported Laminates

As an initial focus, examples are considered for problems which have been studied using an exact approach by Pan (2001), and Pan and Heyliger (2002) for the case of static of simply-supported plates. We first consider a plate with dimensions of $L_x = 0.01$ m and $h = 0.001$ m. The loading is a positive normal traction in the positive z direction on the upper face of the laminate that has the form:

$$t_z = \sin\left(\frac{\pi x}{L_x}\right) \tag{19}$$

All other tractions on the top and bottom surfaces of the laminate are zero, as well as the specified electric displacement and magnetic flux. In this study, we restrict the edge boundary conditions to be consistent with those of geometric simple support (i.e. the transverse displacement w is specified to be zero, with zero normal traction also specified along the edge length). In terms of the electric and magnetic field variables, they are zero along the edges, but nonzero fields can be specified along the top and bottom surfaces of the laminate.

The in-plane approximation functions for each of the five field variables are given in the form:

$$\Gamma_j^u(x) = \cos px \tag{20}$$

$$\Gamma_j^v(x) = \cos px \tag{21}$$

$$\Gamma_j^w(x) = \sin px \tag{22}$$

$$\Gamma_j^\phi(x) = \sin px \tag{23}$$

$$\Gamma_j^\Psi(x) = \sin px \tag{24}$$

where $p = np/L_x$. Here the index j is a single integer that is linked to the numbers used for p in each of the terms. For the loading considered here, only a single term needs to be used to match the exact solution, as the fields with $n = 1$ identically satisfy the (x) dependence of all five field variables. Following this step, all variables depend only on z.

SINGLE-LAYER MAGNETOSTRICTIVE PLATE

The first example considered is a single ply, homogeneous plate of the magnetostrictive $CoFe_2O_4$. The plate is divided into a sequentially higher number of layers starting with 2, then 4, 8, 16, and finally 32. Hence the size of the resulting matrices to be solved are 15, 25, 45, 85 and 165 for these five cases.

The in-plane displacement u is shown in Table 2a as a function of thickness position and number of discrete-layers. The values shown are the maximum quantities for the displacement located at the left edge of the plate ($x = 0$). Because of the nature of the loading, the in-plane displacement u is zero at the plate center. For elementary plate theory, the displacements at the top and bottom surfaces of the plate are identical since the Kirchhoff hypothesis requires that the displacements u and v are linear functions of z. Since the present model is based on an elasticity approach, however, it is seen that there is a slight difference of about 1 % between the values at the top and bottom surfaces of the layer. It is also clear that even for a fairly small number of layers (i.e. 4), the present results are well within 5 percent error of the exact solution values.

The behavior of the transverse displacement w is shown in Table 2b under a similar format. Once again, the present results are in excellent agreement with the exact solution. In elementary plate theory it is common to assume that the displacement field is constant in z (i.e. it does not vary through the thickness). From these results, it is clear that this is not an excessively restrictive assumption, with a difference of less than 0.10 % between values at the top and bottom surfaces. As before, a fairly small number of layers well represents the global plate behavior, with even 4 layers yielding values within 5 % of the exact ones. There is no coupling between the magnetoelastic fields and the electric fields

Table 2. *Maximum displacements and potential for homogeneous magnetostrictive $CoFe_2O_4$ under transverse load.*

z (m)	N = 2	N = 4	N = 8	N = 16	N = 32	Exact
a. In-plane displacement $u(10^{-12}\text{m})$						
0.0000	0.9449	1.0496	1.0798	1.0877	1.0897	1.0903
0.0005	0.0057	0.0057	0.0057	0.0057	0.0057	0.0057
0.0010	−0.9337	−1.0384	−1.0687	−1.0765	−1.0785	−1.0791
b. Transverse displacement $w(10^{-12}\text{m})$						
0.0000	6.1800	6.8392	7.0290	7.0783	7.0907	7.0949
0.0005	6.2289	6.8919	7.0831	7.1328	7.1453	7.1495
0.0010	6.1840	6.8422	7.0319	7.0812	7.0937	7.0978
c. Magnetic vector potential $\psi(10^{-7}\text{C/s})$						
0.0000	−1.8121	−1.6923	−1.6586	−1.6499	−1.6477	−1.6469
0.0005	−2.4400	−2.3767	−2.3593	−2.3548	−2.3537	−2.3533
0.0010	−1.7435	−1.6239	−1.5902	−1.5815	−1.5793	−1.5785

for this problem, and hence the scalar potential is identically equal to zero over the entire thickness. However, the coupling between the elastic and magnetic field results in a nonzero vector potential (and hence magnetic field) through the laminate thickness. This distribution is shown in Table 2c as a function of laminate thickness and number of layers in the approximation. Once again, the agreement is excellent with the exact solution. For this example, the present model yields excellent results for a reasonably small number of layers, and 3 digit accuracy between approaches for 32 layers.

In Figures 1–6, the in-plane normal stresses σ_{xx} and σ_{yy}, the normal stress σ_{zz}, the transverse shear stress σ_{xz}, and the magnetic flux components are shown as a function of laminate thickness for $2, 4, 8, 16$, and 32 layers and are compared with the exact solution by Pan and Heyliger (2002). In each of the sequence of figures

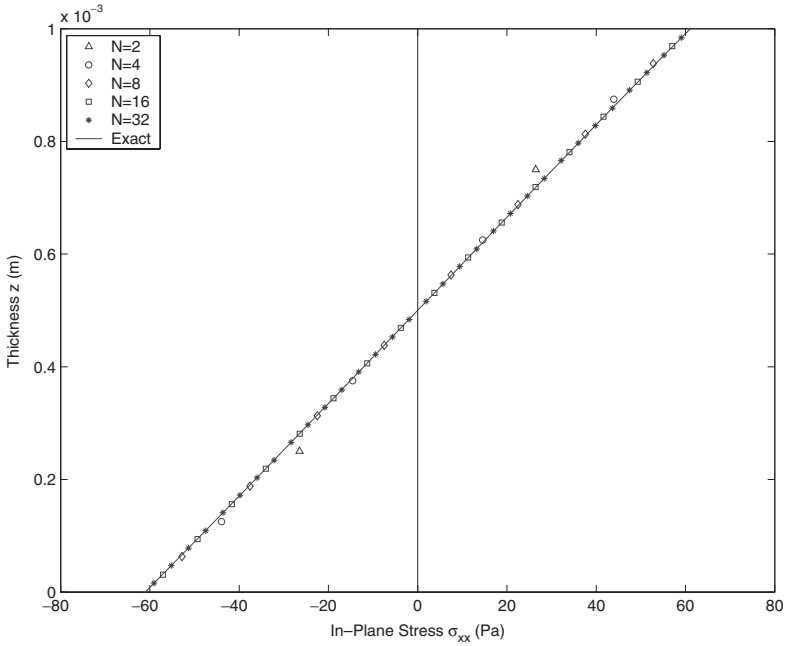

Figure 1. *Variation of stress component σ_{xx} through the laminate thickness for $CoFe_2O_4$ under applied traction.*

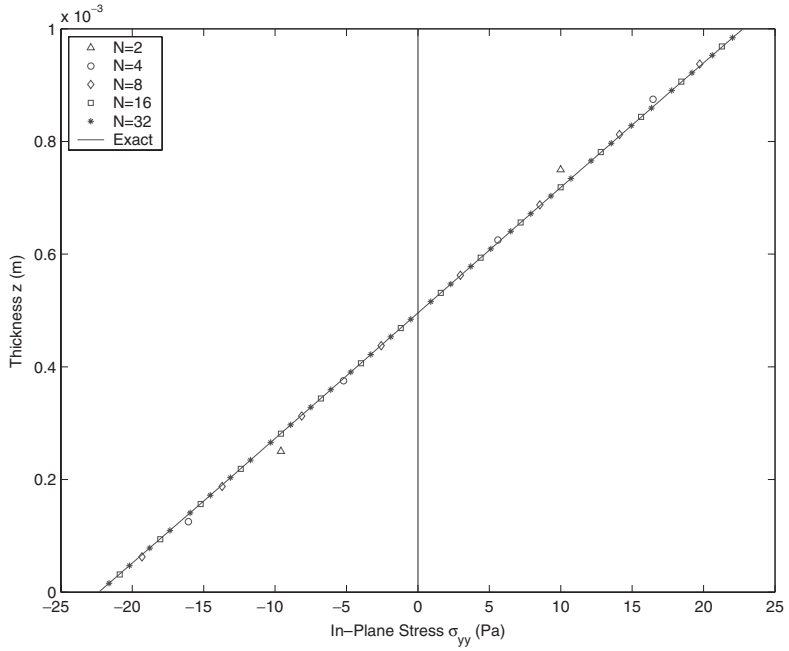

Figure 2. *Variation of stress component σ_{yy} through the laminate thickness for $CoFe_2O_4$ under applied traction.*

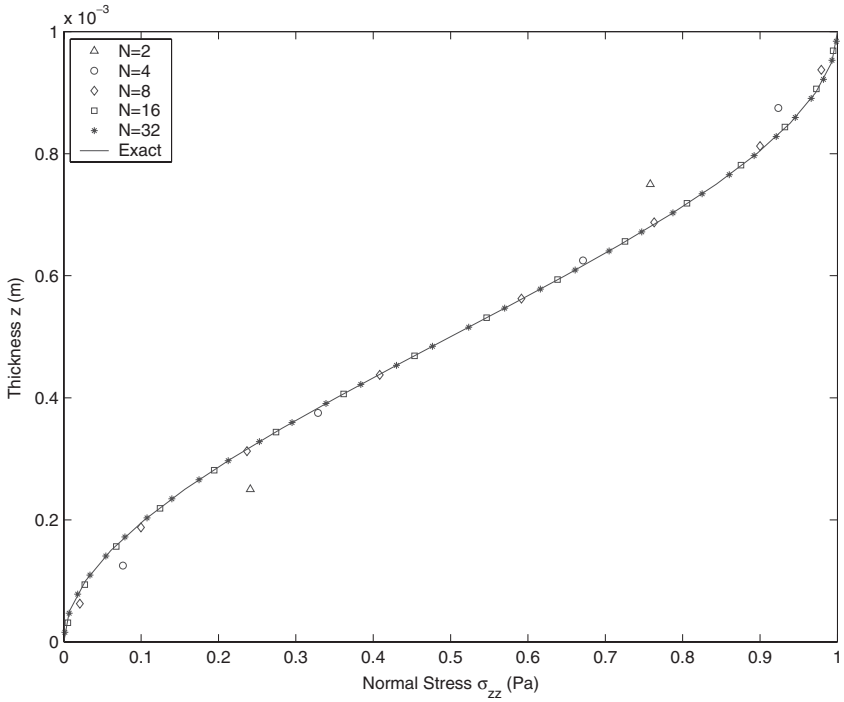

Figure 3. *Variation of stress component σ_{zz} through the laminate thickness for $CoFe_2O_4$ under applied traction.*

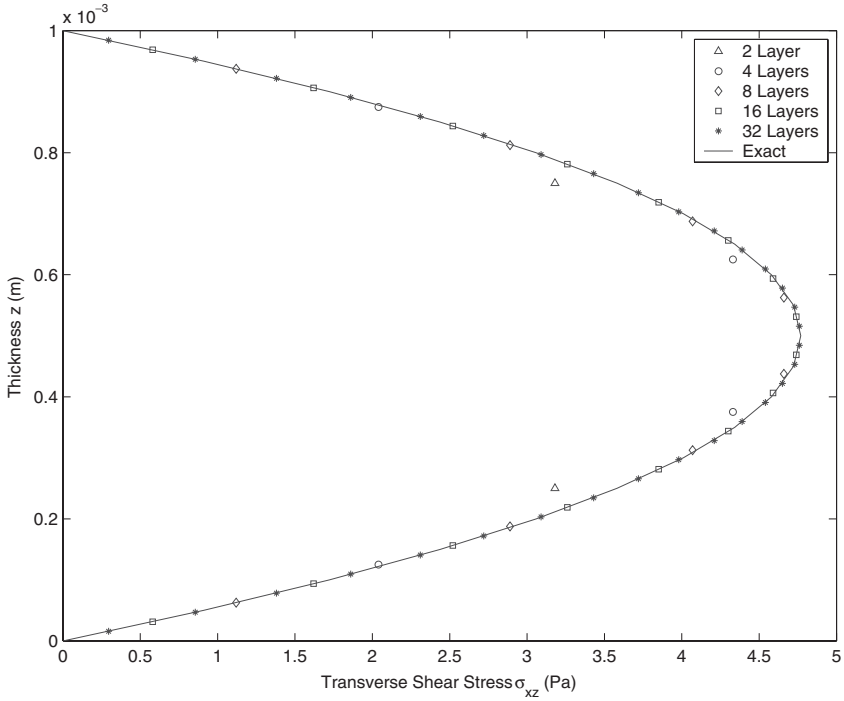

Figure 4. *Variation of stress component σ_{xz} through the laminate thickness for $CoFe_2O_4$ under applied traction.*

that follows, the solid line represents the exact solution, while the open triangles, circles, diamonds, squares, and stars represent the discrete-layer model with $2, 4, 8, 16,$ and 32 layers, respectively. The convergence agreement is clear.

TWO-LAYER COMPOSITE LAMINATE

The second example considered is a two-layer composite laminate formed of the two materials discussed above: the piezoelectric $BaTiO_3$ and the magnetostrictive $CoFe_2O_4$. The laminate geometry is identical

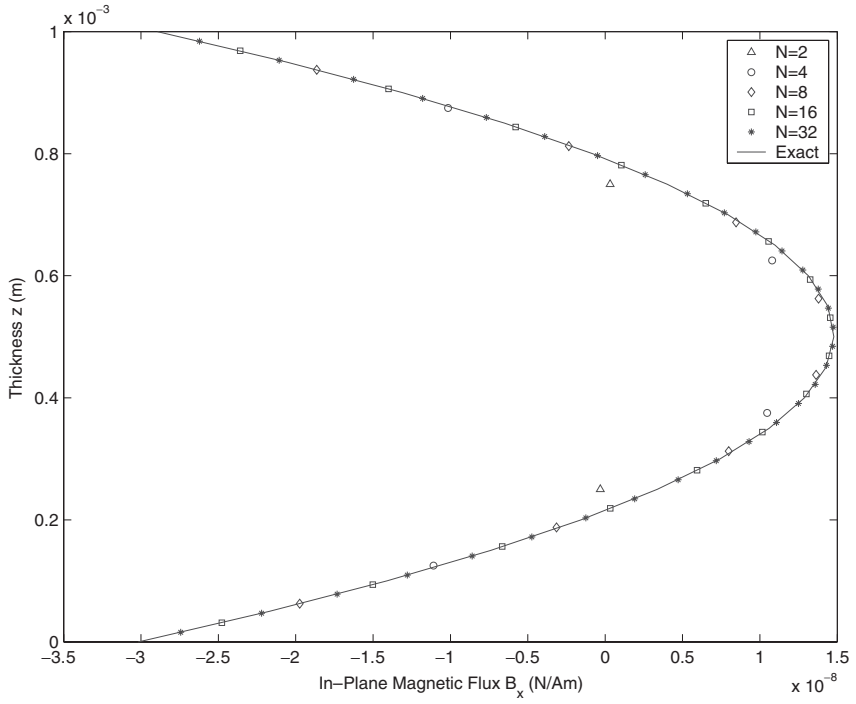

Figure 5. *Variation of magnetic flux component B_x through the laminate thickness for $CoFe_2O_4$ under applied traction.*

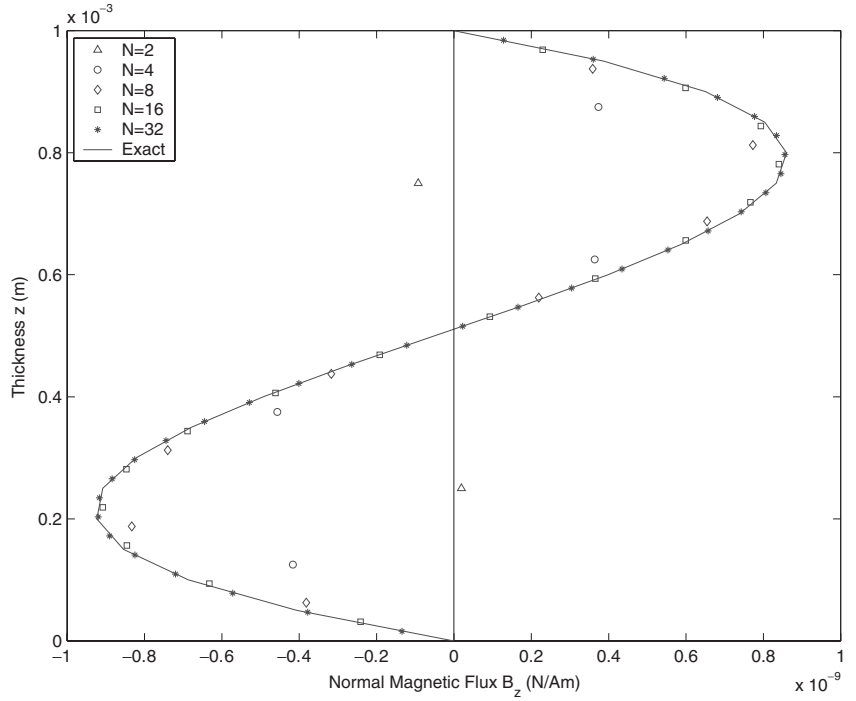

Figure 6. *Variation of magnetic flux component B_z through the laminate thickness for $CoFe_2O_4$ under applied traction.*

to that considered earlier, except that two dissimilar layers are used through the thickness, with equal layer thicknesses used for each lamina. The loading and general form of the boundary conditions and approximation functions are the same as those considered in the previous example.

In Table 3a–d, the in-plane displacement, transverse displacement, electrostatic scalar potential, and magnetic vector potential are shown at the top and bottom surfaces of the laminate and at the interface locations between dissimilar layers as a function of the total number of layers. The value of $N = 2$ is the minimum

Table 3. *Maximum displacements and potential for the two-layer laminate $BaTiO_3/CoFe_2O_4$ under transverse load.*

z (m)	$N=2$	$N=4$	$N=8$	$N=16$	$N=32$	Exact
a. In-plane displacement u (10^{-12} m)						
0.0000	1.0436	1.1267	1.1420	1.1558	1.1573	1.1578
0.0005	−0.0576	−0.0634	−0.0650	−0.0654	−0.0655	−0.0655
0.0010	−1.1720	−1.2636	−1.2891	−1.2957	−1.2973	−1.2979
b. Transverse displacement w (10^{-12} m)						
0.0000	7.2310	7.7784	7.9309	7.9701	7.9799	7.9832
0.0005	7.2807	7.8316	7.9850	8.0244	8.0344	8.0377
0.0010	7.2463	7.7946	7.9473	7.9865	7.9964	7.9997
c. Electrostatic scalar potential ϕ (10^{-4} V)						
0.0000	2.1346	2.1389	2.1404	2.1408	2.1409	2.1410
0.0005	2.1574	2.1616	2.1632	2.1636	2.1637	2.1637
0.0010	1.3134	1.2500	1.2327	1.2283	1.2272	1.2268
d. Magnetic vector potential ψ (10^{-7} C/s)						
0.0000	−1.9834	−1.7744	−1.7172	−1.7026	−1.6989	−1.6977
0.0005	−2.6335	−2.4631	−2.4166	−2.4048	−2.4018	−2.4008
0.0010	−2.6173	−2.4479	−2.4018	−2.3900	−2.3870	−2.3860

number that could be rationally used for this type of structure, as each geometric layer requires at least one discrete-layer to represent the material behavior. The convergence is rapid, and even the magnetic vector potential behavior is well-represented by a relatively small number of layers. Although not shown in these tables, the discrete-layer model has a significant advantage over other types of plate theories in that the requirement of, say, traction continuity (which implies discontinuity of shear strain and therefore through-thickness displacement gradient) is modeled as a matter of course. Allowing the through-thickness approximations to be discontinuous in slope across an interface captures the exact behavior of these fields, frequently leading to more accurate results.

In Figures 7–10, the in-plane normal stresses σ_{xx} and σ_{yy}, the normal stress σ_{zz} and the transverse shear stress σ_{xz} are shown as a function of laminate thickness for $2, 4, 8, 16$, and 32 layers and are compared with the exact solution of Pan and Heyliger (2002). The in-plane normal stress components are discontinuous at the dissimilar layer interface, and hence there is a slight break in magnitude caused by the difference material properties and displacement gradient across the interface. Hence for the laminate, there is an increase in stress consistent with the increase in relative stiffness in going from the $BaTiO_3$ to the $CoFe_2O_4$. The transverse normal and transverse shear stress components are continuous. It is clear from these figures that in terms of stress computation, a small number of layers could be used to accurately represent the behavior of these field components through the thickness, as the results for 4, 8, or 16 discrete layers are in excellent agreement with the exact solution.

In Figures 11–14, the components of the electric displacement and the magnetic flux are shown as a function of laminate thickness for $2, 4, 8, 16$, and 32 layers and are compared with the exact solution of Pan and Heyliger (2002). Here the mismatch in properties is even more significant, as crossing the interface results in going from a piezoelectric medium to a magnetostrictive medium, with the magnetostrictive and piezoelectric coefficients going from zero to nonzero. The field behavior in these two types of layers is very similar because of the nature of the coupling with the electric and magnetic field, and the resulting through-thickness fields reflect this similarity. The normal component of the electric displacement is shown in Figure 12, and the normal component of magnetic flux is shown in Figure 14. Two features of these curves are especially apparent. First, the electric displacement in the magnetostrictive layer and the magnetic flux in the piezoelectric layer are effectively linear. Second, the magnetic flux in the magnetostrictive layer and the electric displacement in the piezoelectric layer are highly nonlinear, with this behavior varying so dramatically that the field quantities given by 2 and 4 discrete layers being very poor approximations of the true field behavior. Only for the case of 8 layers are these quantities well represented and even close to the exact solution. This behavior is in direct contrast to the elastic stress fields, for which even 4 layers gives excellent results. Hence for a laminate with the aspect ratio considered here ($L/t=10$), a minimal number of layers (i.e. 4) may be adequate to represent the three displacement components and the respective stress fields for each layer of the laminate, but at least 8 layers may be required to adequately represent the electric and magnetic potentials flux variables.

TWO-LAYER ANGLE PLY

The piezopolymer polyvinlidene flouride ($PVDF$) is of interest because it is orthotropic, this means that ν, σ_{yz}, σ_{xy}, and D_y are different from zero. A two-layer angle ply $[-45/+45]$ is constructed with the same load and boundary conditions as in the first numerical example, with layer thicknesses $H_1 = H_2 = 0.0005$ m. Results showed excellent agreement with the exact solution by Pan and Heyliger (2002), which is a generalization of the solutions by Heyliger (1994) and Heyliger and Brooks (1996), and they can be seen for the stress components σ_{zz} and σ_{xz}, and for the electrostatic displacement D_z in Figures 15–17.

INFLUENCE OF ASPECT RATIO

In nearly all plate theories, the behavior of the field variables changes dramatically as the plate aspect ratio increases. For elastic laminates, the displacement components tend to approach the kinematic behavior of Kirchhoff plate theory and the stress fields tend to become smooth through the laminate thickness. We investigate this dependence for the two-layer

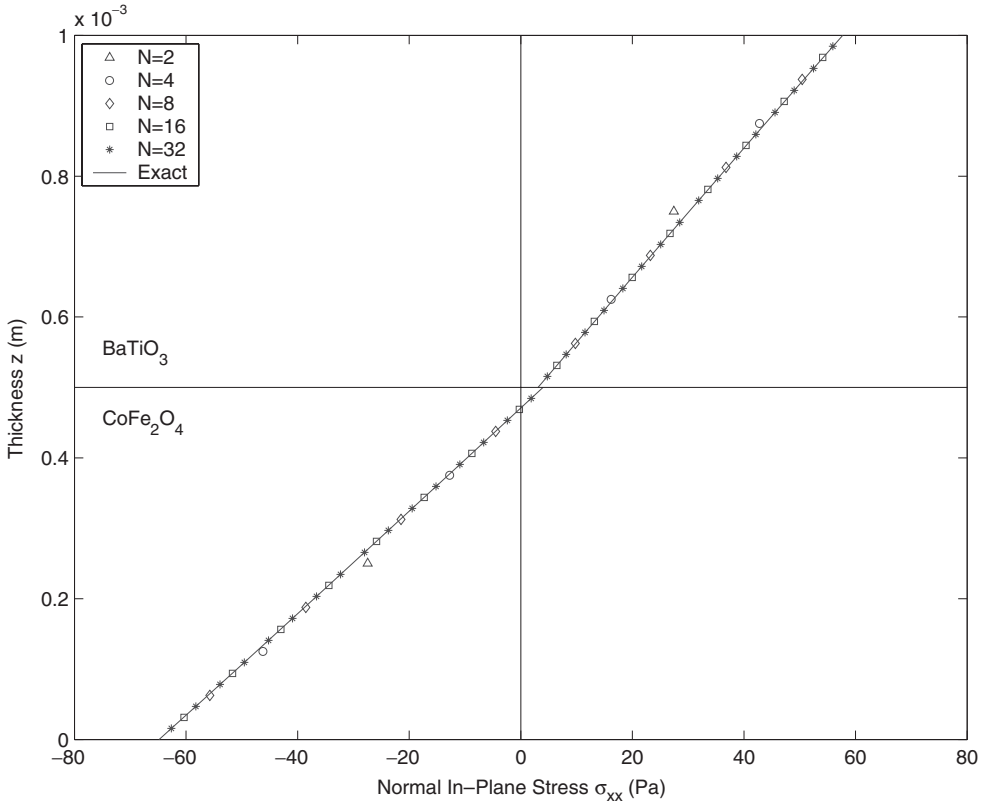

Figure 7. *Variation of stress component σ_{xx} through the laminate thickness for $BaTiO_3/CoFe_2O_4$ under applied traction.*

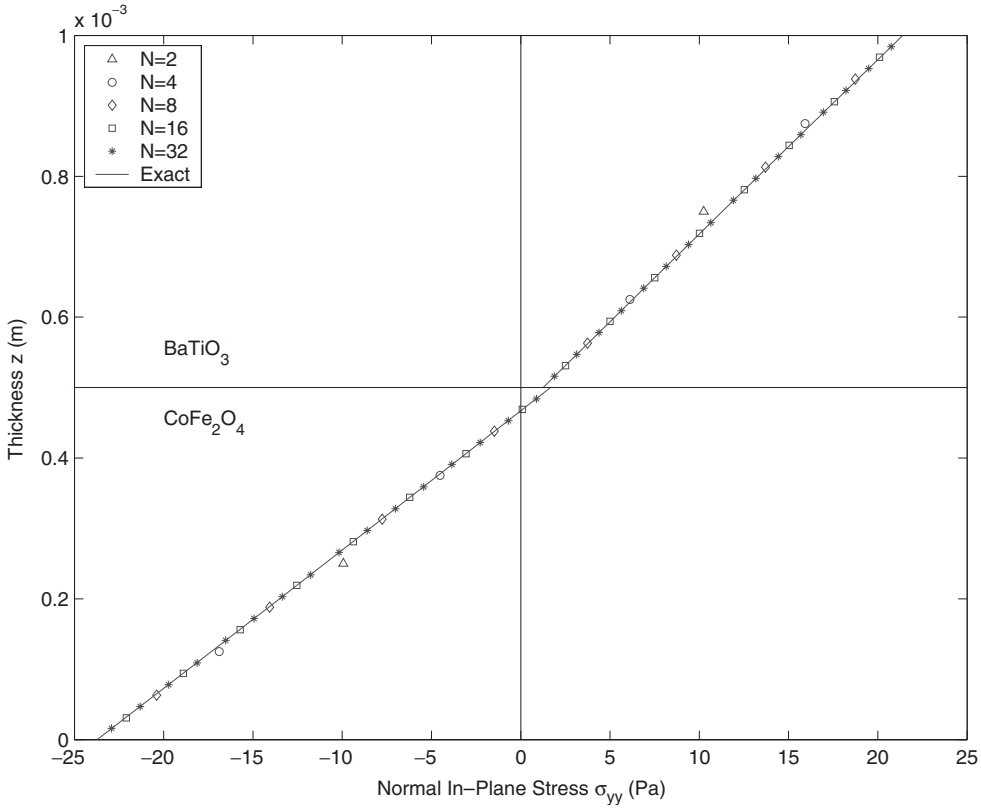

Figure 8. *Variation of stress component σ_{yy} through the laminate thickness for $BaTiO_3/CoFe_2O_4$ under applied traction.*

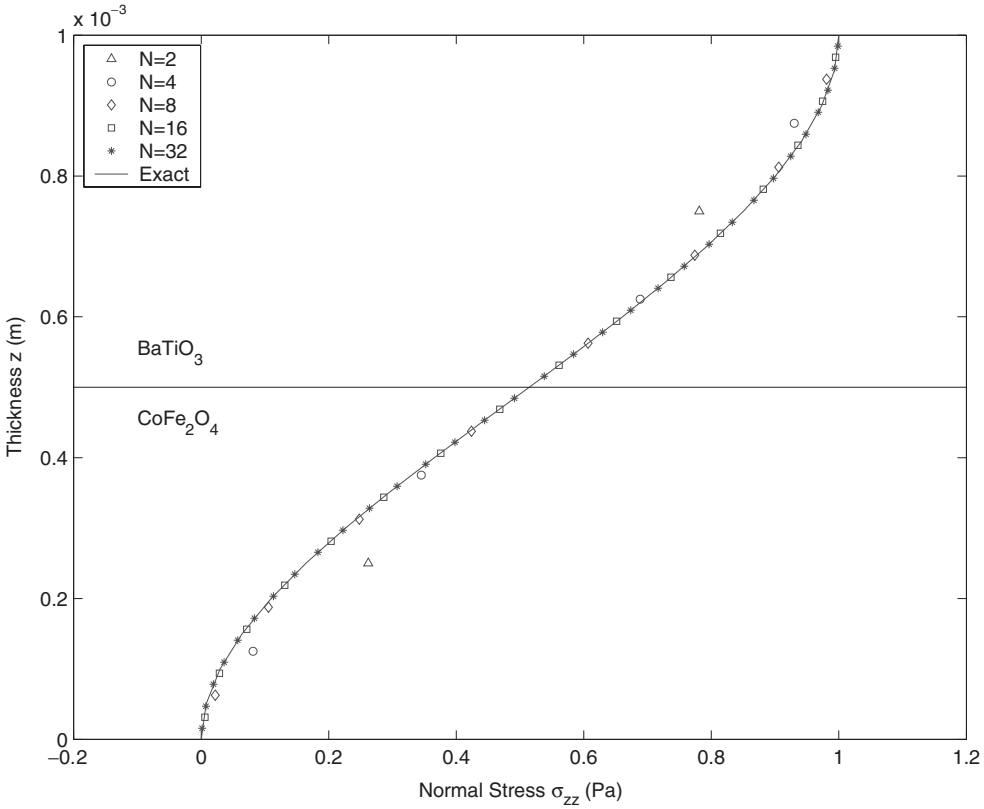

Figure 9. *Variation of stress component σ_{zz} through the laminate thickness for $BaTiO_3/CoFe_2O_4$ under applied traction.*

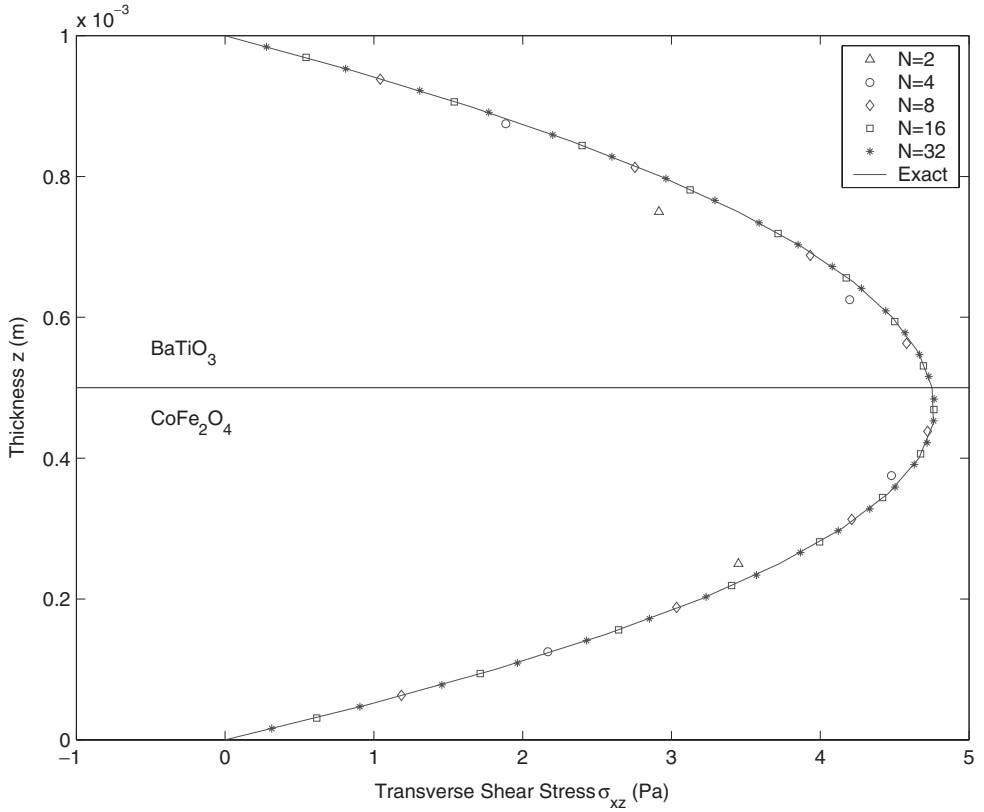

Figure 10. *Variation of stress component σ_{xz} through the laminate thickness for $BaTiO_3/CoFe_2O_4$ under applied traction.*

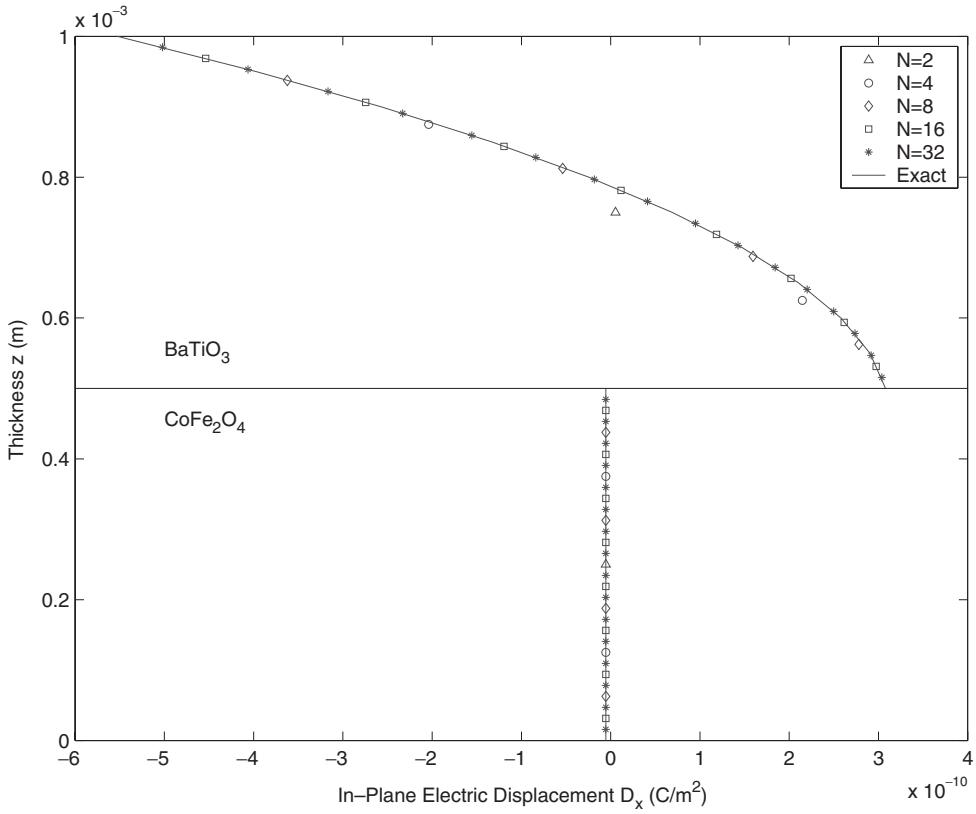

Figure 11. *Variation of electric displacement component D_x through the laminate thickness for $BaTiO_3/CoFe_2O_4$ under applied traction.*

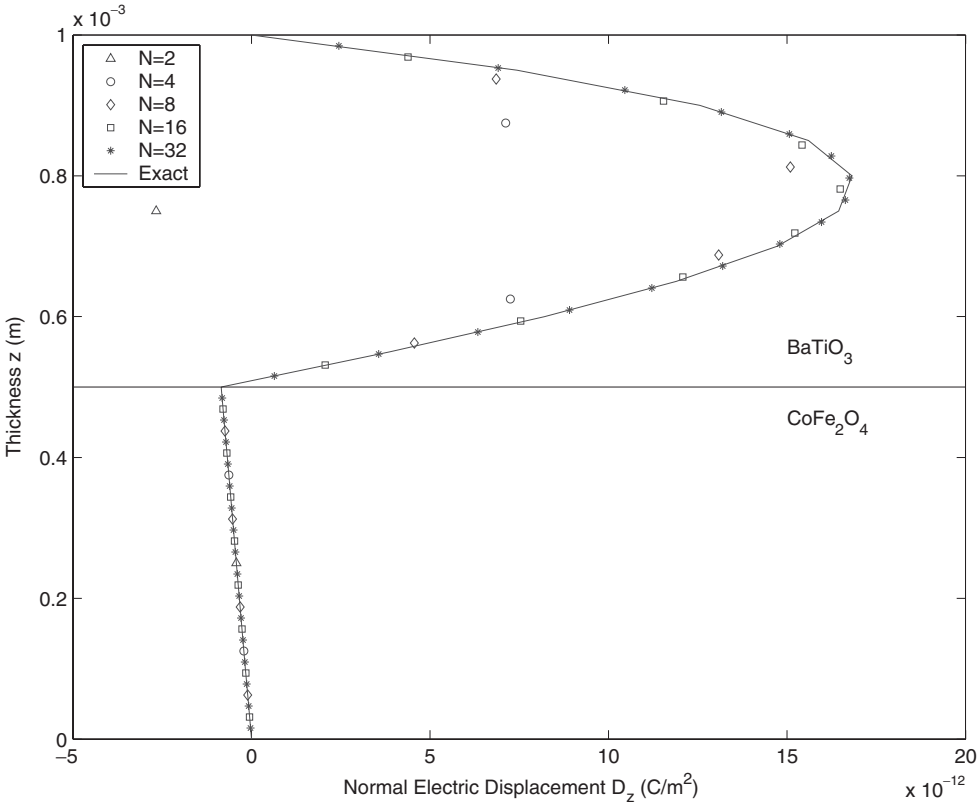

Figure 12. *Variation of electric displacement component D_z through the laminate thickness for $BaTiO_3/CoFe_2O_4$ under applied traction.*

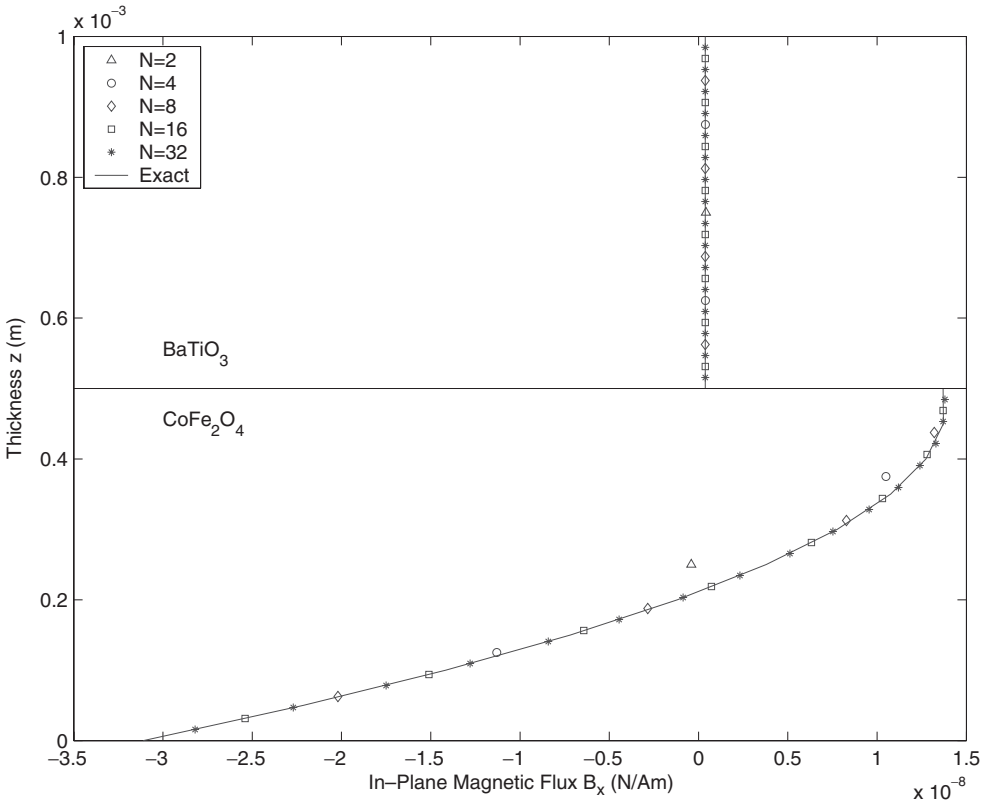

Figure 13. *Variation of magnetic flux component B_x through the laminate thickness for $BaTiO_3/CoFe_2O_4$ under applied traction.*

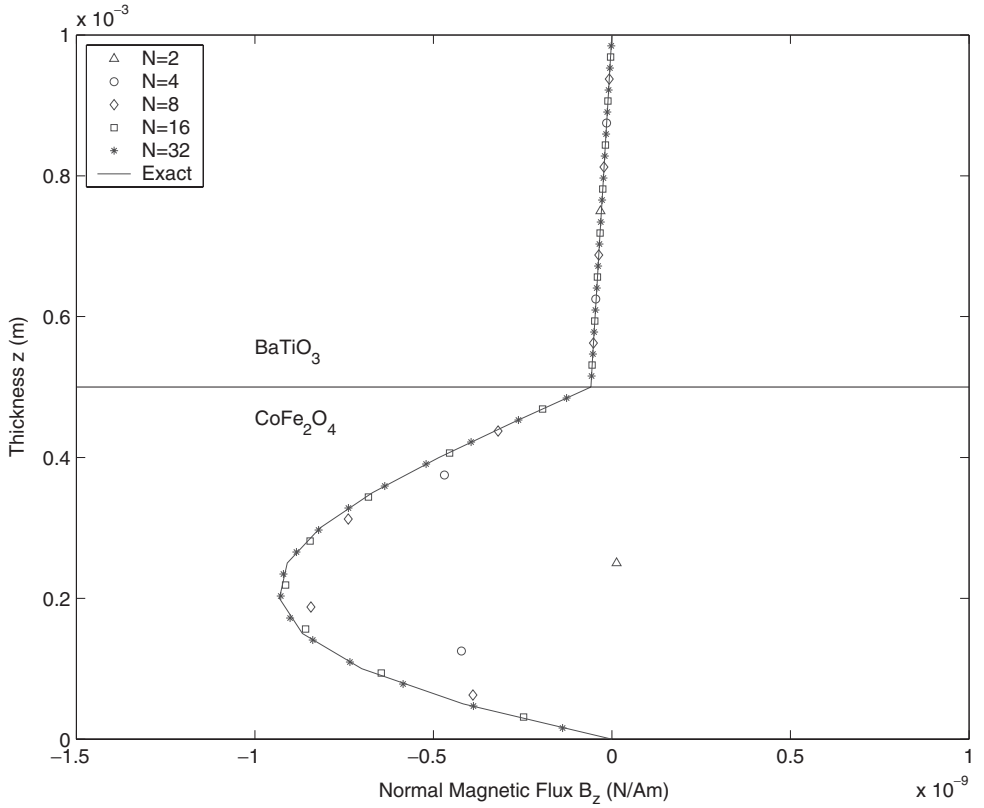

Figure 14. *Variation of magnetic flux component B_z through the laminate thickness for $BaTiO_3/CoFe_2O_4$ under applied traction.*

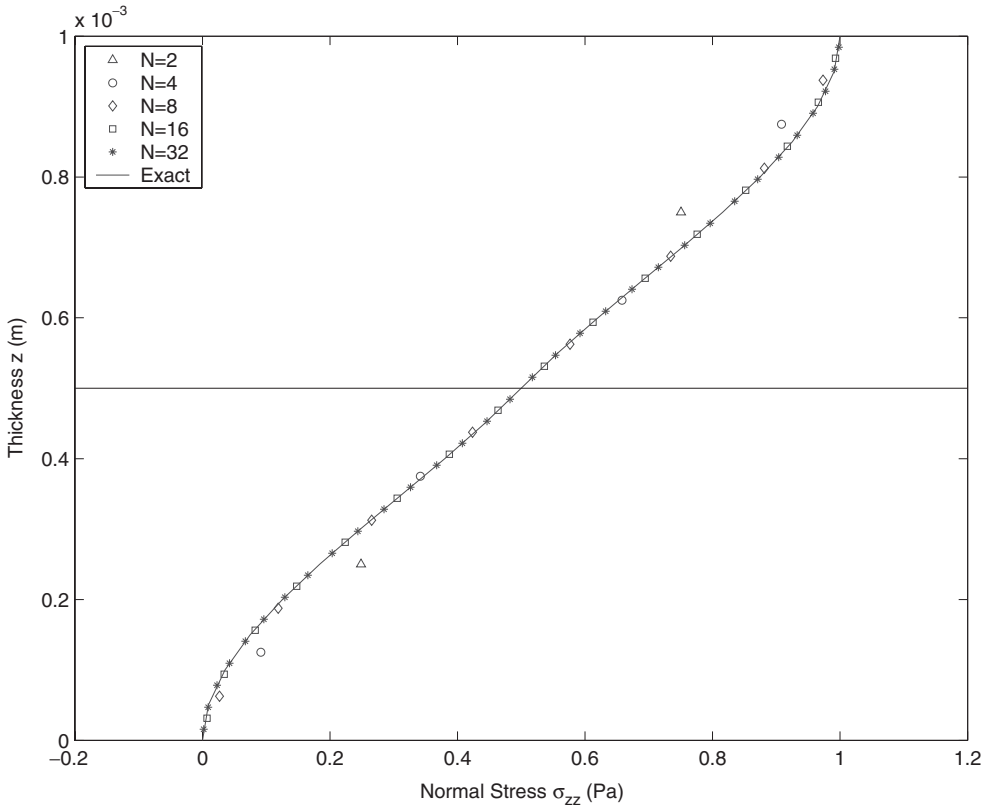

Figure 15. *Variation of stress component σ_{zz} through the laminate thickness for the two-ply [−45/+45] laminate under applied traction.*

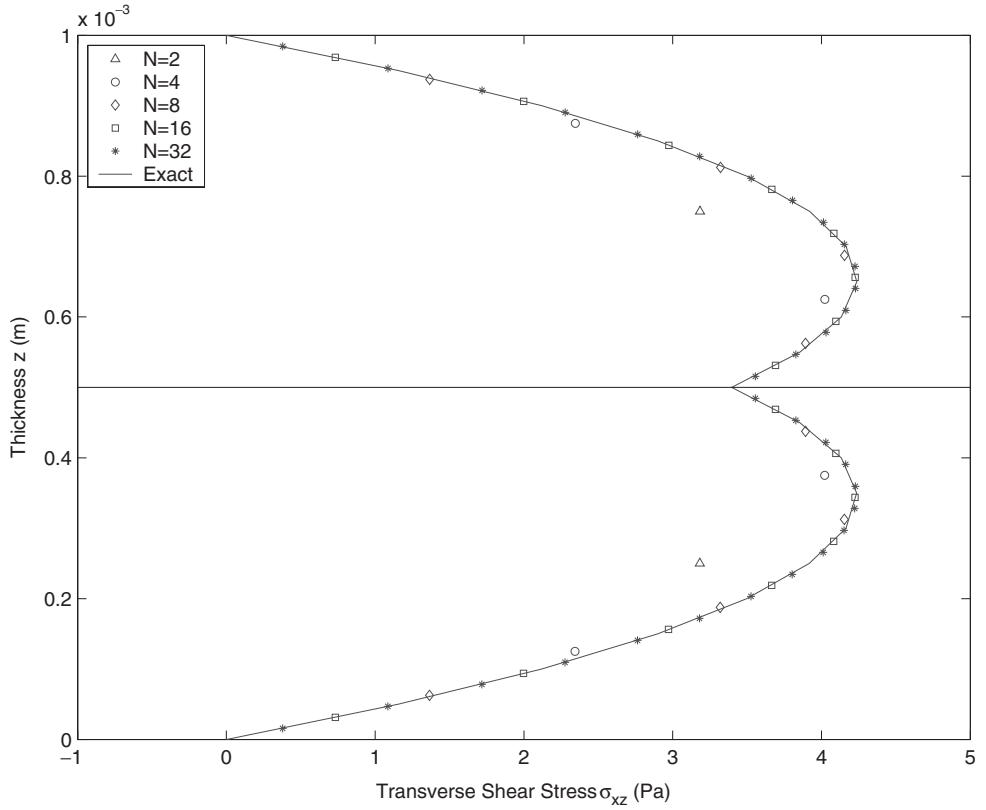

Figure 16. *Variation of stress component σ_{xz} through the laminate thickness for the two-ply [−45/+45] laminate under applied traction.*

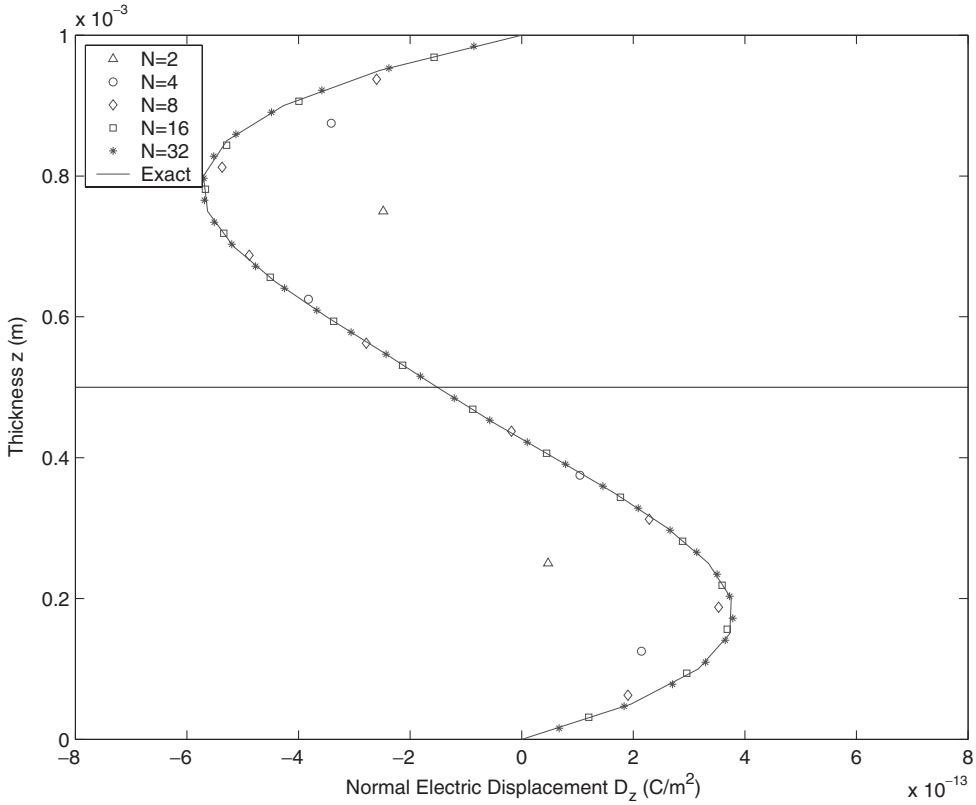

Figure 17. *Variation of electrostatic displacement component D_z through the laminate thickness for the two-ply [−45/+45] laminate under applied traction.*

Table 4. *Maximum elastic displacements and electrostatic potential for the two-ply [−45/+45] laminate under applied traction.*

z	$u \times 10^{-12}$ m		$v \times 10^{-12}$ m		$w \times 10^{-12}$ m		$\phi \times 10^{-4}$ V	
10^{-3} m	DL	Exact	DL	Exact	DL	Exact	DL	Exact
0.000	4.961	4.963	2.070	2.071	3.459	3.460	−4.436	−4.445
0.250	2.412	2.413	2.046	2.047	3.465	3.467	−2.311	−2.319
0.500	0.005	0.005	2.072	2.073	3.467	3.469	−1.718	−1.725
0.750	−2.401	−2.403	2.045	2.045	3.467	3.469	−2.881	−2.889
1.000	−4.953	−4.955	2.069	2.069	3.463	3.465	−5.580	−5.589

magnetoelectroelastic laminate considered in the previous section for the same static loading considered in the previous section. The laminate thickness is fixed as before, but the side lengths of the plate are changed to vary the L/t ratio. Of interest here is the nature of the electrostatic and magnetic potentials as the laminate becomes thin. The field behavior is plotted by normalizing against the maximum value of ϕ or ψ through the laminate thickness for five aspect ratios: 2, 4, 6, 10, and 50. A total of 40 layers (20 per physical layer) are used to compute the fields through the thickness.

The results of these analyses for the electrostatic and magnetic potentials are shown in Figures 18 and 19. The through-thickness characteristics depend strongly on aspect ratio, but quickly tend to a very specific behavior as the aspect ratio increases. There is little change in behavior for $L/t > 10$, and this ratio provides a reasonable estimate on the limiting value where more complex through-thickness field behaviors may be required.

The Completely Free Laminate

A completely traction-free plate is considered with applied surface potential. The intent of this example is to examine the basic deformation characteristics of these simple geometries using the model developed in this study. First, a single layer $BaTiO_3$ laminate with total thickness $h = 0.001\,\text{m}$ and $L_x = 0.01\,\text{m}$ is analyzed. Over the upper surface of the plate, the sinusoidal electrostatic potential is applied, and the bottom and side surfaces of the plate are fixed at zero electrostatic potential. All surfaces of the plate are traction free.

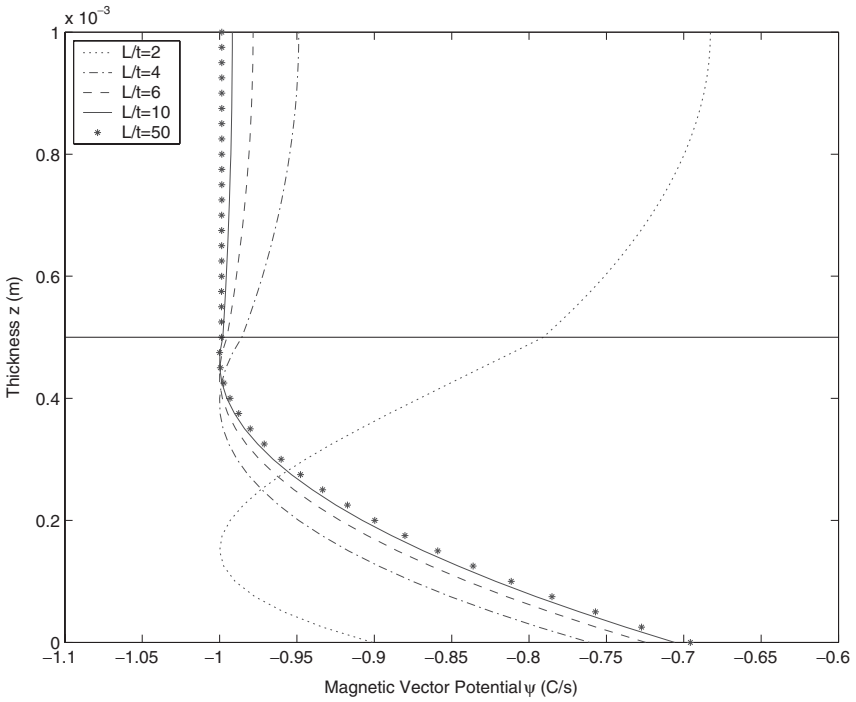

Figure 18. *Through-thickness dependence of electrostatic potential ϕ on laminate aspect ratio for the $BaTiO_3/CoFe_2O_4$ under applied traction.*

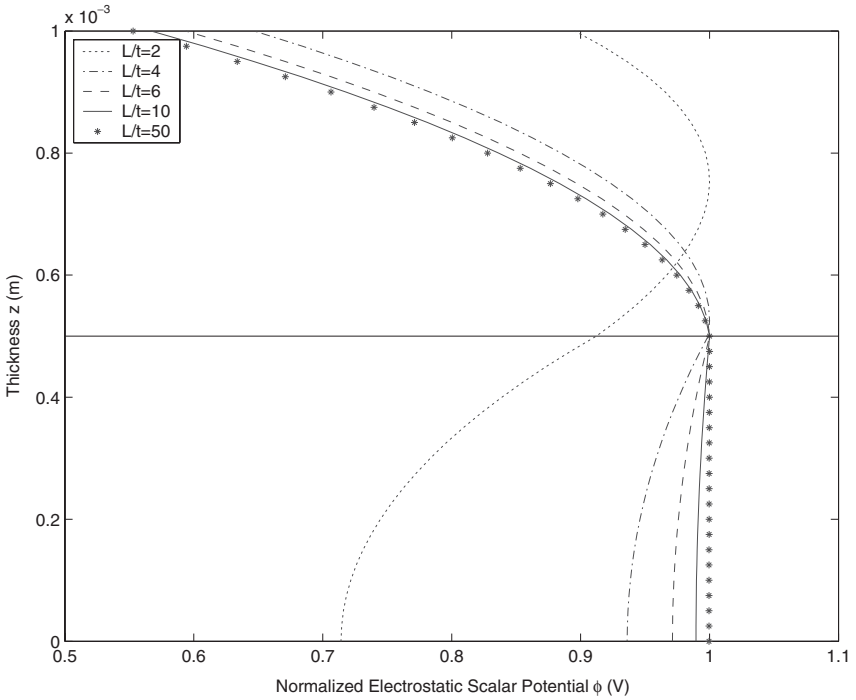

Figure 19. *Through-thickness dependence of magnetic potential ψ on laminate aspect ratio for the $BaTiO_3/CoFe_2O_4$ under applied traction.*

Such a loading is of course more interesting than applying a constant voltage on upper and lower surfaces, which would give constant strains in the x and z directions but no shear strain in the x–z plane. To eliminate the rigid-body modes of the plate, the displacements $u = v = w = \psi = 0$ are specified at the plate center at the middle of the laminate span.

For this loading scenario, the approximation functions are different than those used in the previous section. The in-plane functions for u, v, w, and ψ are selected

as power series in x, with the general form of these functions being given as

$$\Gamma_m = x^m, \tag{25}$$

For the electrostatic potential, we use

$$\Gamma_j^{\phi}(x) = \sin px \tag{26}$$

Since the applied electric field induces symmetric displacements, only odd power series need to be included in the approximation for the u displacement, while even series are required for the w displacement for this specific loading. The through-thickness approximation functions remain as in the previous cases. For the results presented here, six terms are used in the approximations for the displacement components and single trigonometric terms are used for the two potentials. Combined with 32 layers, the final number of unknowns was 999 for the discrete-layer model.

We compare the results with a two-dimensional finite element calculation using 4-node square elements to model half of the plate using symmetry conditions. (This algorithm is briefly described in the Appendix). Thirty elements are used in the length direction and 32 elements are used in the thickness direction, leading to a total of 5115 unknowns for this particular representation. The results of our analysis are shown in Table 5 with the values in the table shown at the left edge of the plate. Very good agreement is found between the two approaches. The largest discrepancy is about 0.6 % difference in the transverse displacement w, with the axial displacements and potential differences nearly achieving 4-digit agreement. The deformed geometry is shown in Figure 20, with the displacements scaled by a factor of 10^6.

We then change the single-layer plate material to the magnetostrictive $CoFe_2O_4$. In this case the laminate is subjected to a sinusoidal magnetic potential on the top surface, with magnetic potential in the bottom surface specified to zero. The approximations functions for the potentials are interchanged, i.e. power series of x are used for the electrostatic potential, and sin px is used for the magnetic potential. Displacements and magnetic potential results are shown in Table 6, and excellent agreement is again found with the FEM results. Figure 21 shows the deformed geometry, using a scaling factor of 10^5.

The bottom of the barium titanate plate remains much flatter than that of the cobalt ferrite. Part of the reason for this is the sign of the coupling coefficient e_{31} compared with q_{31}. In the case of the $BaTiO_3$, this value is negative. At the left end of the laminate, the electric field in the x-direction is negative, leading to a positive normal strain in the z-direction. Hence the lower half of the laminate at the left edge would have a downward motion that partially counteracts the upward movement from the negative shear strain γ_{xz} induced by the q_{15} coupling coefficient. For the $CoFe_2O_4$, the respective coefficient is positive, leading to the opposite effect.

Table 5. *Variation of displacements and electrostatic potential through the laminate thickness for the 1-layer $BaTiO_3$ free laminate under applied electrostatic potential.*

z 10^{-3} m	u – DL 10^{-10} m	u – FEM 10^{-10} m	w – DL 10^{-11} m	w – FEM 10^{-11} m	ϕ – DL V	ϕ – FEM V
0.000	−3.265	−3.266	8.778	8.841	0.000	0.000
0.031	−3.264	−3.265	8.778	8.838	0.031	0.031
0.063	−3.265	−3.265	8.778	8.836	0.062	0.062
0.094	−3.265	−3.265	8.778	8.834	0.092	0.092
0.125	−3.265	−3.265	8.778	8.832	0.123	0.123
0.156	−3.266	−3.266	8.778	8.830	0.154	0.154
0.188	−3.267	−3.267	8.778	8.828	0.185	0.185
0.219	−3.269	−3.268	8.778	8.827	0.216	0.216
0.250	−3.270	−3.270	8.778	8.826	0.247	0.247
0.281	−3.273	−3.272	8.778	8.825	0.277	0.277
0.313	−3.275	−3.274	8.778	8.824	0.308	0.308
0.344	−3.278	−3.277	8.778	8.823	0.339	0.339
0.375	−3.281	−3.280	8.778	8.822	0.370	0.370
0.406	−3.284	−3.283	8.778	8.821	0.401	0.401
0.438	−3.288	−3.287	8.778	8.820	0.432	0.432
0.469	−3.292	−3.291	8.778	8.819	0.463	0.463
0.500	−3.296	−3.295	8.779	8.819	0.495	0.495
0.531	−3.301	−3.300	8.779	8.818	0.526	0.526
0.563	−3.306	−3.305	8.779	8.817	0.557	0.557
0.594	−3.311	−3.310	8.779	8.816	0.588	0.588
0.625	−3.316	−3.315	8.779	8.815	0.619	0.619
0.656	−3.323	−3.321	8.779	8.814	0.651	0.651
0.688	−3.329	−3.328	8.779	8.813	0.682	0.682
0.719	−3.335	−3.334	8.779	8.812	0.714	0.714
0.750	−3.342	−3.341	8.779	8.811	0.745	0.745
0.781	−3.349	−3.348	8.779	8.810	0.777	0.777
0.813	−3.357	−3.356	8.779	8.808	0.809	0.808
0.844	−3.365	−3.364	8.779	8.807	0.840	0.840
0.875	−3.373	−3.372	8.779	8.805	0.872	0.872
0.906	−3.381	−3.381	8.779	8.803	0.904	0.904
0.938	−3.390	−3.390	8.779	8.801	0.936	0.936
0.969	−3.399	−3.399	8.779	8.799	0.968	0.968
1.000	−3.409	−3.409	8.779	8.796	1.000	1.000

Comparing Tables 5 and 6, it can be seen that the axial in-plane deformation, x-direction, caused on the piezoelectric laminate by an applied electrostatic potential is one order of magnitude less than that in the magnetostrictive laminate due to the application of a similar drop in magnitude of the magnetic potential. The difference of deformation in the z-direction is about 50, with the smaller displacement occurring in the piezoelectric laminate. This latter ratio directly corresponds to the ratio of the shear coupling coefficients q_{15} and e_{15}, which provides the change in w along the axis because of the generated axial electric and magnetic fields. For longer plates, of course, this influence would pale in comparison to the usual e_{33} and q_{33} terms, and the deformation would become more uniform along the x-axis of the plate.

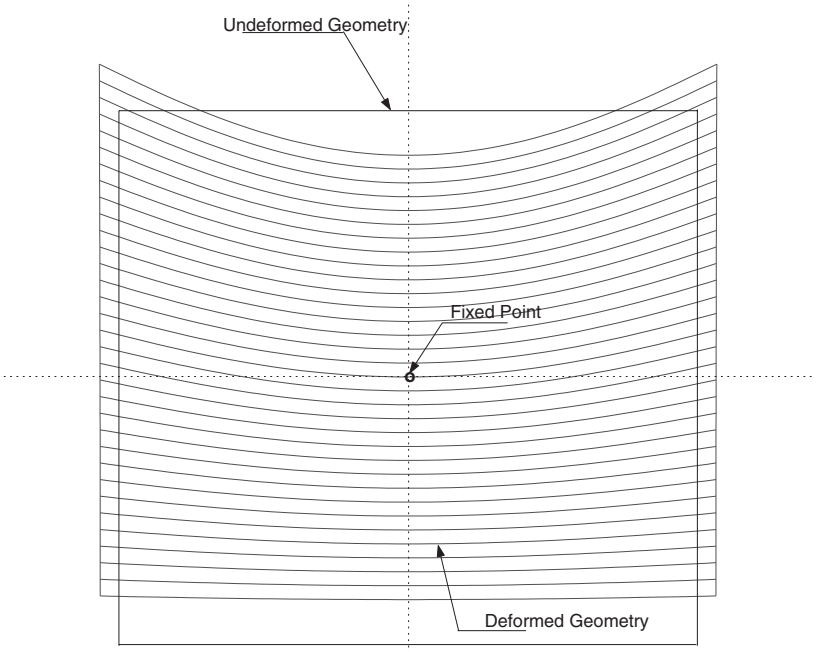

Figure 20. *Deformed shape of the 1-layer $BaTiO_3$ free laminate under applied electrostatic potential.*

Table 6. *Variation of displacements and magnetic potential through the laminate thickness for the 1-layer $CoFe_2O_4$ free laminate under applied magnetic potential.*

z 10^{-3} m	u – DL 10^{-9} m	u – FEM 10^{-9} m	w – DL 10^{-9} m	w – FEM 10^{-9} m	ψ – DL 10^{-9} C/s	ψ – FEM 10^{-9} C/s
0.000	2.423	2.422	4.838	4.846	0.000	0.000
0.031	2.458	2.457	4.838	4.846	0.033	0.033
0.063	2.489	2.488	4.838	4.846	0.066	0.066
0.094	2.518	2.516	4.838	4.847	0.100	0.100
0.125	2.543	2.541	4.838	4.847	0.133	0.133
0.156	2.564	2.563	4.838	4.847	0.166	0.166
0.188	2.583	2.581	4.838	4.848	0.199	0.199
0.219	2.598	2.596	4.838	4.848	0.232	0.232
0.250	2.610	2.608	4.838	4.848	0.265	0.265
0.281	2.619	2.617	4.838	4.848	0.298	0.298
0.313	2.624	2.623	4.839	4.849	0.330	0.330
0.344	2.627	2.625	4.839	4.849	0.363	0.363
0.375	2.626	2.625	4.839	4.849	0.395	0.395
0.406	2.622	2.621	4.839	4.849	0.428	0.428
0.438	2.615	2.614	4.839	4.850	0.460	0.460
0.469	2.605	2.604	4.839	4.850	0.492	0.492
0.500	2.591	2.590	4.840	4.850	0.524	0.524
0.531	2.575	2.574	4.840	4.851	0.555	0.555
0.563	2.555	2.555	4.840	4.851	0.587	0.587
0.594	2.533	2.532	4.840	4.851	0.618	0.618
0.625	2.507	2.507	4.840	4.851	0.649	0.649
0.656	2.479	2.478	4.840	4.852	0.680	0.680
0.688	2.447	2.447	4.840	4.852	0.710	0.710
0.719	2.412	2.412	4.841	4.852	0.740	0.740
0.750	2.375	2.375	4.841	4.852	0.770	0.770
0.781	2.334	2.335	4.841	4.853	0.800	0.800
0.813	2.291	2.291	4.841	4.853	0.830	0.830
0.844	2.245	2.245	4.841	4.853	0.859	0.859
0.875	2.196	2.197	4.841	4.853	0.888	0.888
0.906	2.144	2.145	4.841	4.854	0.916	0.916
0.938	2.089	2.090	4.841	4.854	0.945	0.945
0.969	2.032	2.033	4.841	4.854	0.972	0.972
1.000	1.971	1.974	4.841	4.855	1.000	1.000

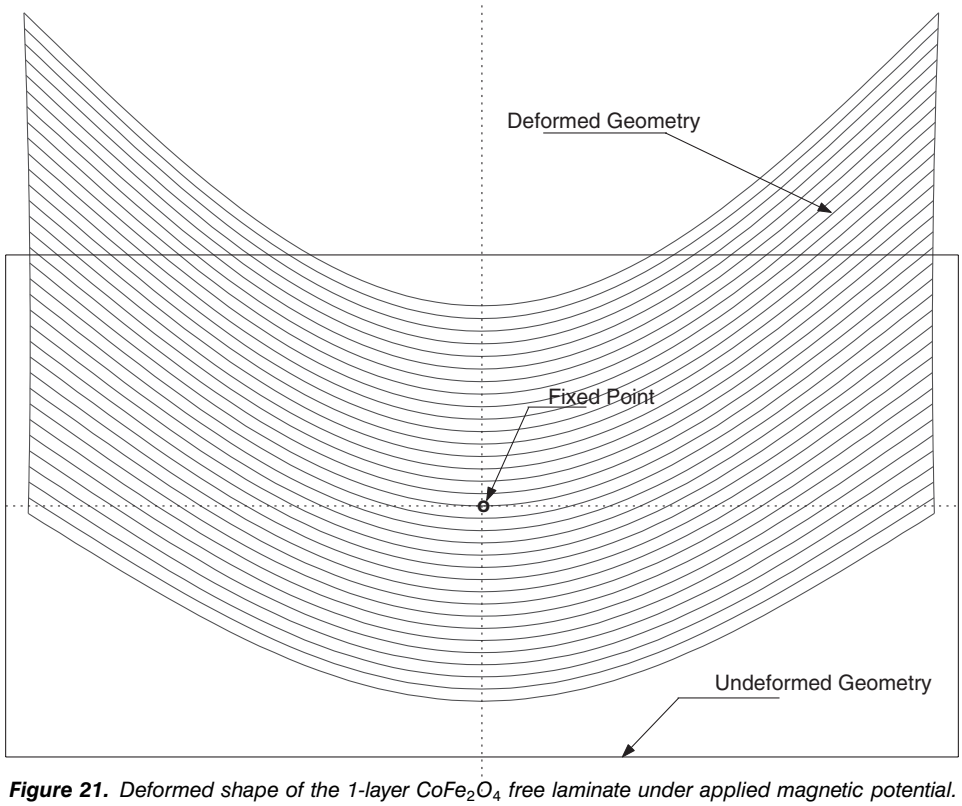

Figure 21. *Deformed shape of the 1-layer $CoFe_2O_4$ free laminate under applied magnetic potential.*

Although we do not present the results of extensive convergence studies, accuracy to within several percent of the values shown here can be obtained with far fewer terms. For example, for only three terms in the power series for displacements, and four discrete-layers along with the single trigonometric term for the potential, a maximum error of only five percent is achieved for w at the lower left corner of the laminate for the piezoelectric laminate, while only 3% is obtained for the magnetostrictive laminate at the same location. Hence this theory could quickly and easily predict estimates for global behavior of numerous materials without the need or cost of typical finite element approximations.

SUMMARY AND CONCLUSIONS

A discrete-layer model has been developed for laminated magnetoelectroelastic plates, and applied to simply-supported laminates in cylindrical bending and single-layer plates under applied electric and magnetic field. Excellent agreement was obtained with exact solutions for the case of cylindrical bending and finite element models for the case of traction-free deformation.

We outline our more significant conclusions below. Although restricted to the laminates considered here using very specific material properties, we expect similar results for other geometries. The two materials considered in this study are readily available and give reasonable numerical predictions, but it is possible that other materials would yield results that fall out of the bounds of the conclusions listed here. Hence we restrict these guidelines for the material properties assumed in this study. Our primary conclusions are:

1. The discrete-layer model can be used to achieve 3–4 digit accuracy in the displacements and potentials with exact solutions for a fairly large number of layers (over 30) using linear basis functions, but accuracy to within several percent can be achieved with around 4 layers for the five primary unknowns.
2. For both homogeneous and layered plates, a reasonably small number of layers (around 5) is required through the thickness to obtain accuracy of several percent for the stress fields. For the electric displacement and electric field distributions, a significantly larger number of layers (around 10) is required for similar accuracy.
3. For aspect ratios over 10, the laminate behavior approaches that of a thin-plate model, and simplified approximations or less layers are likely to yield more accurate comparisons for all unknowns.
4. The global basis functions implicit in the discrete-layer model provide a similar level of accuracy in the primary unknowns over conventional finite elements for studying these solids but reduce the number of unknowns by a factor of about five.

5. For the same potential drop over plate thickness, the magnetostrictive plate under pure magnetic field generates a displacement perpendicular to the axial magnetic field approximately 50 times larger than that of a similar potential drop in electric potential. This is the same ratio of magnitude in shear coefficients q_{15} and e_{15}.

Careful selection of the laminate properties allows for a broad range of behaviors in both electric and magnetic field, raising the possibility of a sensor or actuator with a very broad range of applications. Under time varying inputs, the behaviors could become even more complex since the electric and magnetic fields become more directly linked through the full Maxwell's equations. In addition, there are numerous other issues not considered in this study that are excellent candidates for further study. These include the possibility of mixing orders of approximation for different variables through the thickness, aspect ratio limits for the stress, electric displacements, and magnetic flux variables, and the influence of free edges on the secondary unknowns.

ACKNOWLEDGMENT

The first author gratefully acknowledges the support of the Alexander von Humboldt Foundation in Germany, and the hospitality of Professor Hans Herrmann at the Institute for Computer Applications at the University of Stuttgart.

APPENDIX

Element Stiffness Matrices

The entries in the element coefficients can be expressed as

$$K_{ij}^{uu} = \int_V \left[C_{11} \frac{\partial \Gamma_i^u}{\partial x} \frac{\partial \Gamma_j^u}{\partial x} + C_{55} \frac{\partial \Gamma_i^u}{\partial z} \frac{\partial \Gamma_j^u}{\partial z} \right] dV$$

$$K_{ij}^{uv} = \int_V \left[C_{14} \frac{\partial \Gamma_i^u}{\partial x} \frac{\partial \Gamma_j^v}{\partial z} + C_{45} \frac{\partial \Gamma_i^u}{\partial x} \frac{\partial \Gamma_j^v}{\partial x} + C_{16} \frac{\partial \Gamma_i^u}{\partial z} \frac{\partial \Gamma_j^v}{\partial z} \right] dV$$

$$K_{ij}^{uw} = \int_V \left[C_{13} \frac{\partial \Gamma_i^u}{\partial x} \frac{\partial \Gamma_j^w}{\partial z} + C_{55} \frac{\partial \Gamma_i^u}{\partial z} \frac{\partial \Gamma_j^w}{\partial x} \right] dV$$

$$K_{ij}^{u\phi} = \int_V \left[e_{11} \frac{\partial \Gamma_i^u}{\partial x} \frac{\partial \Gamma_j^\phi}{\partial x} + e_{31} \frac{\partial \Gamma_i^u}{\partial x} \frac{\partial \Gamma_j^\phi}{\partial z} + e_{15} \frac{\partial \Gamma_i^u}{\partial z} \frac{\partial \Gamma_j^\phi}{\partial x} \right] dV$$

$$K_{ij}^{u\psi} = \int_V \left[q_{11} \frac{\partial \Gamma_i^u}{\partial x} \frac{\partial \Gamma_j^\psi}{\partial x} + q_{31} \frac{\partial \Gamma_i^u}{\partial x} \frac{\partial \Gamma_j^\psi}{\partial z} + q_{15} \frac{\partial \Gamma_i^u}{\partial z} \frac{\partial \Gamma_j^\psi}{\partial x} \right] dV$$

$$K_{ij}^{vv} = \int_V \left[C_{44} \frac{\partial \Gamma_i^v}{\partial z} \frac{\partial \Gamma_j^v}{\partial z} + C_{66} \frac{\partial \Gamma_i^v}{\partial x} \frac{\partial \Gamma_j^v}{\partial x} \right] dV$$

$$K_{ij}^{vw} = \int_V \left[C_{45} \frac{\partial \Gamma_i^v}{\partial z} \frac{\partial \Gamma_j^w}{\partial x} + C_{36} \frac{\partial \Gamma_i^v}{\partial x} \frac{\partial \Gamma_j^w}{\partial z} \right] dV$$

$$K_{ij}^{v\phi} = \int_V \left[e_{14} \frac{\partial \Gamma_i^v}{\partial z} \frac{\partial \Gamma_j^\phi}{\partial x} + e_{16} \frac{\partial \Gamma_i^v}{\partial x} \frac{\partial \Gamma_j^\phi}{\partial x} + e_{36} \frac{\partial \Gamma_i^v}{\partial x} \frac{\partial \Gamma_j^\phi}{\partial z} \right] dV$$

$$K_{ij}^{v\psi} = \int_V \left[q_{14} \frac{\partial \Gamma_i^v}{\partial z} \frac{\partial \Gamma_j^\psi}{\partial x} + q_{16} \frac{\partial \Gamma_i^v}{\partial x} \frac{\partial \Gamma_j^\psi}{\partial x} + q_{36} \frac{\partial \Gamma_i^v}{\partial x} \frac{\partial \Gamma_j^\psi}{\partial z} \right] dV$$

$$K_{ij}^{ww} = \int_V \left[C_{33} \frac{\partial \Gamma_i^w}{\partial z} \frac{\partial \Gamma_j^w}{\partial z} + C_{55} \frac{\partial \Gamma_i^w}{\partial x} \frac{\partial \Gamma_j^w}{\partial x} \right] dV$$

$$K_{ij}^{w\phi} = \int_V \left[e_{33} \frac{\partial \Gamma_i^w}{\partial z} \frac{\partial \Gamma_j^\phi}{\partial z} + e_{15} \frac{\partial \Gamma_i^w}{\partial x} \frac{\partial \Gamma_j^\phi}{\partial x} \right] dV$$

$$K_{ij}^{w\psi} = \int_V \left[q_{33} \frac{\partial \Gamma_i^w}{\partial z} \frac{\partial \Gamma_j^\psi}{\partial z} + q_{15} \frac{\partial \Gamma_i^w}{\partial x} \frac{\partial \Gamma_j^\psi}{\partial x} \right] dV$$

$$K_{ij}^{\phi\phi} = \int_V \left[-\epsilon_{11} \frac{\partial \Gamma_i^\phi}{\partial x} \frac{\partial \Gamma_j^\phi}{\partial x} - \epsilon_{33} \frac{\partial \Gamma_i^\phi}{\partial z} \frac{\partial \Gamma_j^\phi}{\partial z} \right] dV$$

$$K_{ij}^{\phi\psi} = \int_V \left[-d_{11} \frac{\partial \Gamma_i^\phi}{\partial x} \frac{\partial \Gamma_j^\psi}{\partial x} - d_{33} \frac{\partial \Gamma_i^\phi}{\partial z} \frac{\partial \Gamma_j^\psi}{\partial z} \right] dV$$

$$K_{ij}^{\psi\psi} = \int_V \left[-\mu_{11} \frac{\partial \Gamma_i^\psi}{\partial x} \frac{\partial \Gamma_j^\psi}{\partial x} - \mu_{33} \frac{\partial \Gamma_i^\psi}{\partial z} \frac{\partial \Gamma_j^\psi}{\partial z} \right] dV$$

Finite Element Model

For the completely free laminate, a comparison is made between the discrete-layer model and a more standard finite element approximation of the three displacements and the two potential functions. In this case, the dependence of the field variables is not separated into the two coordinate functions, but is completed in a more standard way as is usual in finite element methods. Specifically, each of the five field variables are approximated in the form (using the displacement u as an example)

$$u(x, y) = \sum_{j=1}^{4} u_j N_j(x, y) \tag{27}$$

Here the N_j functions are *local* basis functions defined only over an element. This is distinctly different than the discrete-layer model, in which the functions in x

are taken as global basis functions defined over the complete length in x for the laminate and those in z are one-dimensional Lagrangian polynomials.

Substitution of these approximations into the weak form of the governing equations yields an element matrix equation of a similar form to that of Equation (18) for the discrete-layer model. The use of standard finite elements, however, usually implies that the equations are reordered to minimize bandwidth. In addition, as these equations are defined only over an element, conventional methods are used for element assembly into a global system of equations. More details of this sort of approach can be found in Reddy (1984).

REFERENCES

Benveniste, Y. (1995). "Magnetoelectric Effect in Fibrous Composites with Piezoelectric and Piezomagnetic Phases," *Phys. Rev. B*, 51: 16424–16427.

Berlincourt, D.A., Curran, D.R. and Jaffe, H. (1964). Physical Acoustics, 1, *Piezoelectric and Piezomagnetical Materials and their Function in Transducers*, 169–270.

Harshe, G., Dougherty, J.P. and Newnham, R.E. (1993). "Theoretical Modeling of Multilayer Magnetoelectric Composites," *Int. J. Appl. Electromag.*, 4:145–159.

Heyliger, P. (1994). "Static Behavior of Laminated Elastic/Piezoelectric Plates," *AIAA J.*, 32:2481–2484.

Heyliger, P.R., and Brooks, S.P. (1996). "Exact Solutions for Piezoelectric Laminates in Cylindrical Bending," *J. Appl. Mech.*, 64:903–910.

Nan, C.W. (1994). "Magnetoelectric Effect in Composites of Piezoelectric and Piezomagnetic Phases," *Phys. Rev. B*, B50: 6082–6088.

Pan, E. (2001). "Exact Solution for Simply Supported and Multilayered Magneto-Electro-Elastic Plates," *J. Appl. Mech.*, 68:608–618.

Pan, E., and Heyliger, P.R. (2002). "Free Vibrations of Simply-Supported and Multilayered Magneto-Electro-Elastic Plates," *J. Sound Vibr.*, 252:429–442.

Pan, E., and Heyliger, P.R. (2003). "Exact Solutions for Magneto-electroelastic Laminates in Cylindrical Bending," *Int. J. Sol. Struc.*, 40:6859–6876.

Pauley, K.E., and Dong, S.B. (1976). "Analysis of Plane Waves in Laminated Piezoelectric Media, Wave Electronics," 1:265–285.

Reddy, J.N. (1984). *Energy and Variational Methods in Applied Mechanics*, John Wiley and Sons, New York.

Reddy, J.N. (1987). "A Generalization of Displacement-based Laminate Theories, Communications in Applied Numerical Methods," 3:173–181.

Saravanos, D.A. and Heyliger, P.R. (1999). "Mechanics and Computational Models for Laminated Piezoelectric Beams, Plates, and Shells," *Appl. Mech. Rev.*, 52:305–320.

Tashiro, K., Tadokoro, H. and Kobayashi, M. (1981). "Structure and Piezoelectricity of Poly(Vinylidene Flouride)," *Ferroelectrics*, 32:167–175.

Tzou, H.S. (1993). *Piezoelectric Shells: Distributed Sensing and Control of Continua*, Kluwer Academic, Norwell, MA.